

Range-separated tensor format for numerical modeling of many-particle interaction potentials

Peter Benner ^{*} Venera Khoromskaia ^{**} Boris N. Khoromskij [◇]

Abstract

We introduce and analyze the new range-separated (RS) canonical/Tucker tensor format which aims for numerical modeling of the 3D long-range interaction potentials in multi-particle systems. The main idea of the RS tensor format is the independent grid-based low-rank representation of the localized and global parts in the target tensor which allows the efficient numerical approximation of N -particle interaction potentials. The single-particle reference potential like $1/\|x\|$ is split into a sum of localized and long-range low-rank canonical tensors represented on a fine 3D $n \times n \times n$ Cartesian grid. The smoothed long-range contribution to the total potential sum is represented on the 3D grid in $O(n)$ storage via the low-rank canonical/Tucker tensor. We prove that the Tucker rank parameters depend only logarithmically on the number of particles N and the grid-size n . Agglomeration of the short range part in the sum is reduced to an independent treatment of N localized terms with almost disjoint effective supports, calculated in $O(N)$ operations. Thus, the cumulated sum of short range clusters is parametrized by a single low-rank canonical reference tensor with a local support, accomplished by a list of particle coordinates and their charges. The RS canonical/Tucker tensor representations reduce the cost of multi-linear algebraic operations on the 3D potential sums arising in modeling of multi-dimensional data by radial basis functions, say, in computation of the electrostatic potential of a protein, in 3D integration and convolution transforms, computation of gradients, forces and the interaction energy of a many-particle systems, and in low parametric fitting of multi-dimensional scattered data by reducing all of them to 1D calculations.

Key words: Low-rank tensor decompositions, summation of electrostatic potentials, long-range many-particle interactions, canonical and Tucker tensor formats, Ewald summation.

AMS Subject Classification: 65F30, 65F50, 65N35, 65F10

1 Introduction

Numerical treatment of long-range potentials is a challenging task in computer modeling of dynamics and structure of multiparticle systems, for example, in molecular dynamics

^{*}Max Planck Institute for Dynamics of Complex Systems, Sandtorstr. 1, D-39106 Magdeburg, Germany (benner@mpi-magdeburg.mpg.de)

^{**}Max Planck Institute for Mathematics in the Sciences, Leipzig; Max Planck Institute for Dynamics of Complex Systems, Magdeburg (vekh@mis.mpg.de).

[◇]Max Planck Institute for Mathematics in the Sciences, Inselstr. 22-26, D-04103 Leipzig, Germany (bokh@mis.mpg.de).

simulations of large solvated biological systems like proteins, in analysis of periodic Coulombic systems or scattered data in geosciences, Monte Carlo sampling etc. [54, 19, 32, 57, 49, 24]. For a given non-local generating kernel $p(\|x\|)$, $x \in \mathbb{R}^3$, the calculation of a weighted sum of interaction potentials in the large N -particle system, with the particle locations at $x_\nu \in \mathbb{R}^3$, $\nu = 1, \dots, N$,

$$P(x) = \sum_{\nu=1}^N Z_\nu p(\|x - x_\nu\|), \quad Z_\nu \in \mathbb{R}, \quad x_\nu, x \in \Omega = [-b, b]^3, \quad (1.1)$$

leads to computationally intensive numerical task. Indeed, the generating radial basis function $p(\|x\|)$ is allowed to have a slow polynomial decay in $1/\|x\|$ as $\|x\| \rightarrow \infty$ so that each individual term in (1.1) contributes essentially to the total potential at each point in the computational domain Ω , thus predicting the $O(N)$ complexity for the straightforward summation at every fixed target $x \in \mathbb{R}^3$. Moreover, in general, the function $p(\|x\|)$ has a singularity or a cusp at the origin, $x = 0$, making its full grid representation problematic. Typical examples of the radial basis functions $p(\|x\|)$ are given by the Newton $1/\|x\|$, Slater $e^{-\lambda\|x\|}$, Yukawa/Helmholtz $e^{-\lambda\|x\|}/\|x\|$ and other Green's kernels (see examples in §4.1).

The traditional approaches based on the Ewald summation method [23] combined with the fast Fourier transform (FFT) usually apply to calculation of the interaction energy or the interparticle forces of a system of N -particles with the periodic closure, which reduces the complexity scaling in a particle number from $O(N^2)$ to $O(N \log N)$ [19, 20]. These approaches need meshing up the result of Ewald sums over 3D Cartesian grid for the charge assignment onto a $n_m \times n_m \times n_m$ mesh. Generation of the smoothed charge distribution on the right-hand side of the arising Poisson's equation is the main complexity limitation since it requires the N -term summation of the grid functions of size $O(n_m^3)$, presuming the dominating cost $O(n_m^3 N)$. This procedure is accomplished by the cheap FFT solver with periodic boundary conditions that amounts to $O(n_m^3 \log n_m)$ operations.

The mesh implementation approaches trace back to the original so-called particle-particle-particle-mesh (P³M) methods [31].

The fast multipole expansion [27] method allows to compute some characteristics of the multi-particle potential, say, the interaction energy, at the expense $O(N \log N)$ by evaluation of the potential only at N sampling points x_ν .

Computation of long-range interaction potentials of large many-particle systems is discussed for example in [15, 46, 54], and using grid-based approaches in [31, 1, 19, 20, 60, 25]. Ewald-type splitting of the Coulomb interaction into long- and short-range components was applied in density functional theory calculations [59].

In this paper, we introduce and analyze the new range-separated (RS) canonical/Tucker tensor format which aims for the efficient numerical treatment of 3D long-range interaction potentials in a system of rather generally distributed particles. The main idea of the RS format is the independent grid-based low-rank tensor representation to the long- and short-range parts in the total sum of single-particle (say, electrostatic) potentials in (1.1) discretized on a fine 3D $n \times n \times n$ Cartesian grid Ω_n in the computational box $\Omega \in \mathbb{R}^3$. Such a representation is based on the splitting of a single reference potential like $p(\|x\|) = 1/\|x\|$ into a sum of localized and long-range low-rank canonical tensors both represented on the computational grid Ω_n .

The main advantage of the RS format is efficient representation of the long-range contributions to the total potential sum in (1.1) by using the multigrid accelerated canonical-to-Tucker

transform [42], which returns this part in a form of a low-rank canonical/Tucker tensor at the asymptotical cost $O(Nn)$. In Theorem 3.2, we prove that the corresponding tensor rank only weakly (logarithmically) depends on the number of particles N . Hence, the long-range contribution to the target sum is represented via the low-rank global canonical/Tucker tensor defined on the fine $n \times n \times n$ grid Ω_n , in the $O(n)$ storage. These features are demonstrated by numerical tests for the large 3D clusters of generally distributed particles.

In turn, the short-range contribution to the total sum is constructed by using a *single* reference low-rank tensor of local support selected from the "short-range" canonical vectors in the tensor decomposition of the radial basis function $p(\|x\|)$. To that end the whole set of N short-range clusters is represented by replication and rescaling of the small-size localized canonical tensor defined on an $n_s \times n_s \times n_s$ Cartesian grid with $n_s \ll n$, thus reducing the storage to the $O(1)$ -parametrization of the reference canonical tensor and the list of coordinates and charges of particles. Summation of the short-range part over $n \times n \times n$ grid needs $O(Nn_s)$ computational work for N -particle system. Such cumulated sum of the short-range components allows "local operations" in the RS-canonical format, making it particularly efficient for tensor multilinear algebra.

The particular benefit of the RS approach is the low-parametric representation of the collective interaction potential on a large 3D Cartesian grid in the whole computational domain Ω at the linear cost $O(n)$, thus outperforming the traditional grid-based summation techniques based on the full-grid $O(n^3)$ -representation in the volume. Both global and local summation schemes are quite easy in program implementation. The prototype algorithms in MATLAB[®] applied on a laptop allow to compute the RS-tensor representation of electrostatic potential for large many-particle systems on fine grids of size up to $n^3 = 10^{12}$.

The efficient numerical realization of RS formats can be achieved by a trade off between the rank parameters in the long-range part and the effective support of the local sub-tensors. Indeed, the range separation step can be realized *adaptively* by a simple tuning of splitting rank parameters in the reference tensor based on an ε -tolerance threshold in estimating the effective local support. The low-rank RS canonical/Tucker tensor representation simplifies further operations on the resultant interaction potential, for example, 3D integration, computation of gradients and forces, or evaluation of the interaction energy of a system by reducing all of them to 1D calculations.

As one of many possible applications of the RS tensor format, we propose a new numerical scheme for calculation of the free interaction energy of proteins, and the enhanced regularized formulation for solving the Poisson-Boltzmann equation (PBE) that models the electrostatic potential of proteins in a solvent. We also demonstrate that the RS tensor formats can be useful in numerical modeling of the multi-dimensional scattered data by means of the efficient data sparse approximation to the "inter-distance" matrix via the short term sum of Kronecker product matrices with the "univariate" factors.

The RS tensor format was motivated by the recent method for efficient summation of the long-range electrostatic potentials on large lattices with defects by using the assembled canonical and Tucker tensors [36, 38], which provides a competitive alternative to the Ewald summation schemes [23]. In case of 3D finite lattice systems, the grid-based tensor summation technique yields asymptotic complexity $O(N^{1/3})$ in the number of particles N , and almost linear complexity in the univariate grid-size n .

The RS-tensor approach can be interpreted as the model reduction based on the low-rank

tensor approximations (i.e., via a small number of representation parameters). The model reduction techniques for PDEs and control problems were described in detail in [6, 55, 4].

In the recent years, the tensor numerical methods have been recognized as a powerful tool in scientific computing for multidimensional problems, see for example [41, 26, 37, 5, 2] and [18, 17, 56, 45, 29, 12, 3, 21]. In particular, the approximating properties of tensor decompositions in modeling of high-dimensional problems have been addressed in [58, 10, 28, 14]. Here we notice that in the case of higher dimensions the local canonical tensors can be combined with the global low-rank tensor train (TT) representation [53] thus introducing the RS-TT format, see Remark 3.13.

The rest of the paper is organized as follows. In Section 2, we introduce the canonical and Tucker tensor formats, and provide a description of the short-long range splitting to the canonical tensor approximation of the Newton kernel by using sinc-quadratures applied to the Laplace transform. Section 2 also discusses the principles for selection of the short and long-range parts in the reference electrostatic potential. Grid-based tensor splitting of the electrostatic potential sums is addressed in Section 3, where the efficient computation of the long-range part of the potential is described. In particular, Section 3.3 introduces and analyses the classes of range-separated tensor formats. The possible application to protein modeling is addressed in Section 4. Furthermore, we discuss how the RS tensor formats may be utilized in the numerical treatment of multi-dimensional scattered data, for calculation of gradients, forces and interaction energy of the system. Appendix recalls the main ingredients of the reduced HOSVD tensor approximation and the canonical-to-Tucker tensor transform applied in the numerical implementations.

2 Range separated tensor form of a reference potential

2.1 Representation of multivariate functions via low-rank tensors

In this section we recall the commonly used rank-structured tensor formats¹ utilized in this paper (see also the literature surveys [44, 41, 26]). The traditional canonical and Tucker tensor representations were long since known in computer science for the quantitative analysis of correlations in the multidimensional data arising in image processing, chemometrics, psychometrics etc., see [16, 44] and references therein.

These formats have attracted the attention of the scientific computation community when it was recently shown numerically and rigorously proved that in most cases function related tensors allow low-rank tensor decomposition [39, 35]. In particular, they proved to be efficient for real-space calculations in computational quantum chemistry [36, 37].

A tensor of order d is defined as a multidimensional array over a d -tuple index set,

$$\mathbf{A} = [a_{i_1, \dots, i_d}] \equiv [a(i_1, \dots, i_d)] \in \mathbb{R}^{n_1 \times \dots \times n_d} \quad \text{with} \quad i_\ell \in I_\ell := \{1, \dots, n_\ell\},$$

considered as an element of a linear vector space equipped with the Euclidean scalar product. Tensors with all dimensions having equal size $n_\ell = n$, $\ell = 1, \dots, d$, will be called an $n^{\otimes d}$ tensor.

¹ The commonly used notion *rank-structured tensor formats* for the compressed representation of multidimensional data is usually understood in sense of the (nonlinear) parametrization by a small number of parameters that allows low storage costs, a simple representation of each entry in the target data array, and the efficient "formatted" multilinear algebra via reduction to univariate operations.

The required storage size scales exponentially in the dimension, n^d , which results in the so-called "curse of dimensionality".

To get rid of exponential scaling in the dimension, one can apply the rank-structured separable representations (approximations) of multidimensional tensors. The simplest separable element is given by the rank-1 tensor,

$$\mathbf{U} = \mathbf{u}^{(1)} \otimes \dots \otimes \mathbf{u}^{(d)} \in \mathbb{R}^{n_1 \times \dots \times n_d},$$

with entries $u_{i_1, \dots, i_d} = u_{i_1}^{(1)} \dots u_{i_d}^{(d)}$, requiring only $n_1 + \dots + n_d$ numbers to store it. A tensor in the R -term canonical format is defined by a finite sum of rank-1 tensors,

$$\mathbf{U} = \sum_{k=1}^R \xi_k \mathbf{u}_k^{(1)} \otimes \dots \otimes \mathbf{u}_k^{(d)}, \quad \xi_k \in \mathbb{R}, \quad (2.1)$$

where $\mathbf{u}_k^{(\ell)} \in \mathbb{R}^{n_\ell}$ are normalized vectors, and R is called the canonical rank of a tensor. Now the storage cost is bounded by dRn . For $d \geq 3$, there are no algorithms for computation of the canonical rank of a tensor \mathbf{U} , i.e. the minimal number R in representation (2.1) and the respective decomposition with the polynomial cost in d .

We say that a tensor \mathbf{V} is represented in the rank- \mathbf{r} orthogonal Tucker format with the rank parameter $\mathbf{r} = (r_1, \dots, r_d)$, if

$$\mathbf{V} = \sum_{\nu_1=1}^{r_1} \dots \sum_{\nu_d=1}^{r_d} \beta_{\nu_1, \dots, \nu_d} \mathbf{v}_{\nu_1}^{(1)} \otimes \dots \otimes \mathbf{v}_{\nu_d}^{(d)}, \quad \ell = 1, \dots, d, \quad (2.2)$$

where $\{\mathbf{v}_{\nu_\ell}^{(\ell)}\}_{\nu_\ell=1}^{r_\ell} \in \mathbb{R}^{n_\ell}$, represents a set of orthonormal vectors for $\ell = 1, \dots, d$, and $\boldsymbol{\beta} = [\beta_{\nu_1, \dots, \nu_d}] \in \mathbb{R}^{r_1 \times \dots \times r_d}$ is the Tucker core tensor. The storage cost for the Tucker tensor is bounded by $d r n + r^d$, with $r = |\mathbf{r}| := \max_\ell r_\ell$.

In the case $d = 2$, the orthogonal Tucker decomposition is equivalent to the singular value decomposition (SVD) of a rectangular matrix.

An equivalent notation for the Tucker tensor format can be used,

$$\mathbf{V} = \boldsymbol{\beta} \times_1 V^{(1)} \times_2 V^{(2)} \dots \times_d V^{(d)}, \quad (2.3)$$

where \times_ℓ denotes the contraction along the mode ℓ and orthogonal matrices $V^{(\ell)} = [\mathbf{v}_1^{(\ell)} \dots \mathbf{v}_{r_\ell}^{(\ell)}] \in \mathbb{R}^{n_\ell \times r_\ell}$ incorporate the set of orthogonal vectors $\{\mathbf{v}_{\nu_\ell}^{(\ell)}\}$. Likewise, the representation (2.1) can be written as the rank- (R, \dots, R) (non-orthogonal) Tucker tensor

$$\mathbf{U} = \boldsymbol{\xi} \times_1 U^{(1)} \times_2 U^{(2)} \dots \times_d U^{(d)}, \quad (2.4)$$

by introducing the so-called side matrices $U^{(\ell)} = [\mathbf{u}_1^{(\ell)} \dots \mathbf{u}_R^{(\ell)}] \in \mathbb{R}^{n_\ell \times R}$, $\ell = 1, \dots, d$, obtained by concatenation of the canonical vectors $\mathbf{u}_k^{(\ell)}$, $k = 1, \dots, R$, and the diagonal Tucker core tensor $\boldsymbol{\xi} := \text{diag}\{\xi_1, \dots, \xi_R\} \in \mathbb{R}^{R \times \dots \times R}$ such that $\xi_{\nu_1, \dots, \nu_d} = 0$ except when $\nu_1 = \dots = \nu_d$ with $\xi_{\nu, \dots, \nu} = \xi_\nu$ ($\nu = 1, \dots, R$).

The exceptional properties of the Tucker decomposition for the approximation of discretized multidimensional functions have been revealed in [39, 35], where it was proven that for a class of function-related tensors the approximation error of the Tucker decomposition decays exponentially in the Tucker rank.

Rank-structured tensor representations provide fast multilinear algebra with linear complexity scaling in the dimension d . For example, for given canonical tensors (2.1), the Euclidean scalar product, the Hadamard product and d -dimensional convolution can be computed by simple tensor operations in $1D$ complexity [35]. In tensor-structured numerical methods, calculation of the d -dimensional convolution integrals is replaced by a sequence of $1D$ scalar and Hadamard products, and $1D$ convolution transforms [42, 35], leading to $O(dn \log n)$ computational work instead of $O(n^d)$. However, the multilinear tensor operations in the above mentioned formats mandatory lead to increase of tensor ranks which can be then reduced by the canonical-to-Tucker and Tucker-to-canonical algorithms introduced in [35, 42], see Appendix for the description of the canonical-to-Tucker algorithm.

2.2 Canonical tensor representation of the 3D Newton kernel

Methods of separable approximation to the 3D Newton kernel (electrostatic potential) using the Gaussian sums have been addressed in the chemical and mathematical literature since [9] and [58, 10, 28], respectively. The approach to tensor decomposition for a class of lattice-structured interaction potentials $p(\|x\|)$ was presented in [36, 38]. In this section, we recall the grid-based method for the low-rank canonical representation of a spherically symmetric kernel function $p(\|x\|)$, $x \in \mathbb{R}^d$ for $d = 1, 2, 3$, by its projection onto the set of piecewise constant basis functions, see [7] for the case of Newton and Yukawa kernels $p(\|x\|) = \frac{1}{\|x\|}$, and $p(\|x\|) = \frac{e^{-\lambda\|x\|}}{\|x\|}$, for $x \in \mathbb{R}^3$. The single reference potential like $1/\|x\|$ can be represented on a fine 3D $n \times n \times n$ Cartesian grid in the form low-rank canonical tensor [28, 7].

In the computational domain $\Omega = [-b, b]^3$, let us introduce the uniform $n \times n \times n$ rectangular Cartesian grid Ω_n with mesh size $h = 2b/n$ (n even). Let $\{\psi_{\mathbf{i}}\}$ be a set of tensor-product piecewise constant basis functions, $\psi_{\mathbf{i}}(\mathbf{x}) = \prod_{\ell=1}^3 \psi_{i_\ell}^{(\ell)}(x_\ell)$, for the 3-tuple index $\mathbf{i} = (i_1, i_2, i_3)$, $i_\ell \in \{1, \dots, n\}$, $\ell = 1, 2, 3$. The generating kernel $p(\|x\|)$ is discretized by its projection onto the basis set $\{\psi_{\mathbf{i}}\}$ in the form of a third order tensor of size $n \times n \times n$, defined entry-wise as

$$\mathbf{P} := [p_{\mathbf{i}}] \in \mathbb{R}^{n \times n \times n}, \quad p_{\mathbf{i}} = \int_{\mathbb{R}^3} \psi_{\mathbf{i}}(x) p(\|x\|) \, dx. \quad (2.5)$$

The low-rank canonical decomposition of the 3rd order tensor \mathbf{P} is based on using exponentially convergent sinc-quadratures for approximation of the Laplace-Gauss transform to the analytic function $p(z)$, $z \in \mathbb{C}$, specified by a certain weight $a(t) > 0$,

$$p(z) = \int_{\mathbb{R}_+} a(t) e^{-t^2 z^2} \, dt \approx \sum_{k=-M}^M a_k e^{-t_k^2 z^2} \quad \text{for } |z| > 0, \quad z \in \mathbb{R}, \quad (2.6)$$

where the quadrature points and weights are given by

$$t_k = k \mathfrak{h}_M, \quad a_k = a(t_k) \mathfrak{h}_M, \quad \mathfrak{h}_M = C_0 \log(M)/M, \quad C_0 > 0. \quad (2.7)$$

Under the assumption $0 < a \leq |z| < \infty$ this quadrature can be proven to provide an exponential convergence rate in M for a class of analytic functions $p(z)$, see [58, 28]. In particular, for the Newton kernel, $p(z) = 1/z$, the Laplace-Gauss transform takes the form

$$\frac{1}{z} = \frac{2}{\sqrt{\pi}} \int_{\mathbb{R}_+} e^{-z^2 t^2} \, dt, \quad \text{where } z = \sqrt{x_1^2 + x_2^2 + x_3^2}.$$

Now, for any fixed $x = (x_1, x_2, x_3) \in \mathbb{R}^3$, such that $\|x\| > a > 0$, we apply the sinc-quadrature approximation (2.6), (2.7) to obtain the separable expansion

$$p(\|x\|) = \int_{\mathbb{R}_+} a(t) e^{-t^2 \|x\|^2} dt \approx \sum_{k=-M}^M a_k e^{-t_k^2 \|x\|^2} = \sum_{k=-M}^M a_k \prod_{\ell=1}^3 e^{-t_k^2 x_\ell^2}, \quad (2.8)$$

providing an exponential convergence rate in M ,

$$\left| p(\|x\|) - \sum_{k=-M}^M a_k e^{-t_k^2 \|x\|^2} \right| \leq \frac{C}{a} e^{-\beta \sqrt{M}}, \quad \text{with some } C, \beta > 0. \quad (2.9)$$

Combining (2.5) and (2.8), and taking into account the separability of the Gaussian basis functions, we arrive at the low-rank approximation to each entry of the tensor \mathbf{P} ,

$$p_i \approx \sum_{k=-M}^M a_k \int_{\mathbb{R}^3} \psi_i(x) e^{-t_k^2 \|x\|^2} dx = \sum_{k=-M}^M a_k \prod_{\ell=1}^3 \int_{\mathbb{R}} \psi_{i_\ell}^{(\ell)}(x_\ell) e^{-t_k^2 x_\ell^2} dx_\ell.$$

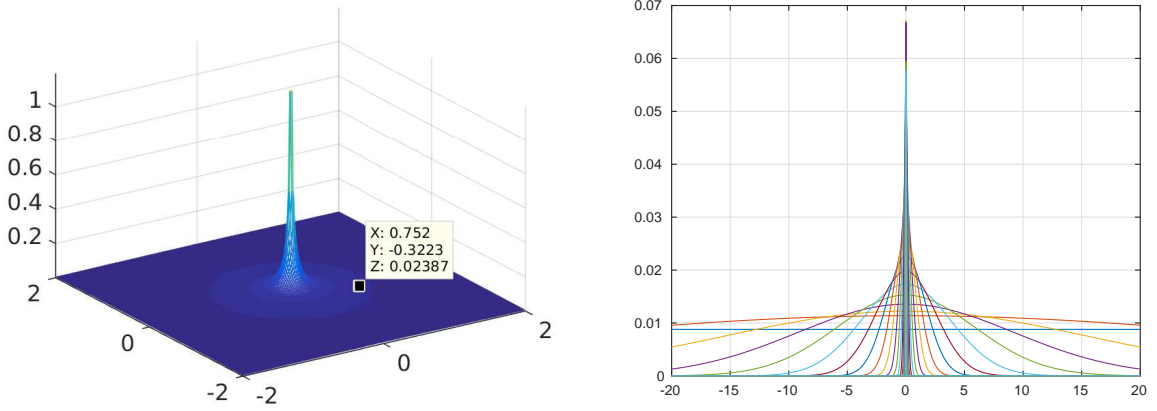


Figure 2.1: Vectors of the canonical tensor representation, $\{\mathbf{p}_q^{(1)}\}_{q=1}^R$, for the Newton kernel displayed along x -axis: $n = 1024$, $R = 20$.

Define the vector (recall that $a_k > 0$)

$$\mathbf{p}_k^{(\ell)} = a_k^{1/3} \left[b_{i_\ell}^{(\ell)}(t_k) \right]_{i_\ell=1}^{n_\ell} \in \mathbb{R}^{n_\ell} \quad \text{with} \quad b_{i_\ell}^{(\ell)}(t_k) = \int_{\mathbb{R}} \psi_{i_\ell}^{(\ell)}(x_\ell) e^{-t_k^2 x_\ell^2} dx_\ell,$$

then the 3rd order tensor \mathbf{P} can be approximated by the R -term ($R = 2M + 1$) canonical representation

$$\mathbf{P} \approx \mathbf{P}_R = \sum_{k=-M}^M a_k \bigotimes_{\ell=1}^3 \mathbf{b}^{(\ell)}(t_k) = \sum_{k=-M}^M \mathbf{p}_k^{(1)} \otimes \mathbf{p}_k^{(2)} \otimes \mathbf{p}_k^{(3)} \in \mathbb{R}^{n \times n \times n}, \quad \mathbf{p}_k^{(\ell)} \in \mathbb{R}^{n_\ell}. \quad (2.10)$$

Given a threshold $\varepsilon > 0$, M can be chosen as the minimal number such that in the max-norm

$$\|\mathbf{P} - \mathbf{P}_R\| \leq \varepsilon \|\mathbf{P}\|.$$

The skeleton vectors can be re-numerated by $k \mapsto q = k + M + 1$, $\mathbf{p}_k^{(\ell)} \mapsto \mathbf{p}_q^{(\ell)}$, ($q = 1, \dots, R$), $\ell = 1, 2, 3$. The canonical tensor \mathbf{P}_R in (2.10) approximates the 3D symmetric kernel function $p(\|x\|)$ ($x \in \Omega$), centered at the origin, such that $\mathbf{p}_q^{(1)} = \mathbf{p}_q^{(2)} = \mathbf{p}_q^{(3)}$ ($q = 1, \dots, R$).

In the case of the Newton kernel the term $\mathbf{p}_k^{(\ell)}$ equals $\mathbf{p}_{-k}^{(\ell)}$, and the sum (2.10) reduces to $k = 0, 1, \dots, M$, implying $R = M + 1$. Figure 2.1 displays the canonical vectors in the tensor representation (2.10) for the Newton kernel along the x -axis from a set $\{\mathbf{p}_q^{(1)}\}_{q=1}^R$. It is clearly seen that there are canonical vectors representing the long- and short-range contributions to the total electrostatic potential. This interesting feature was also recognized for the rank-structured tensors representing a lattice sum of potentials [36, 38].

2.3 Tensor splitting of the kernel into long- and short-range parts

From the definition of the quadrature (2.10), (2.7), we can easily observe that the full set of approximating Gaussians includes two classes of functions: those with small "effective support" and the long-range functions. Clearly, functions from different classes may require different tensor-based schemes for their efficient numerical treatment. Hence, the idea of the new approach is the constructive implementation of a range separation scheme that allows the independent efficient treatment of both the long- and short-range parts in the approximating kernel.

In the following, without loss of generality, we confine ourselves to the case of the Newton kernel, so that the sum in (2.10) reduces to $k = 0, 1, \dots, M$ (due to symmetry argument). From (2.7) we observe that the sequence of quadrature points $\{t_k\}$, can be split into two subsequences,

$$\mathcal{T} := \{t_k | k = 0, 1, \dots, M\} = \mathcal{T}_l \cup \mathcal{T}_s,$$

with

$$\mathcal{T}_l := \{t_k | k = 0, 1, \dots, R_l\}, \quad \text{and} \quad \mathcal{T}_s := \{t_k | k = R_l + 1, \dots, M\}. \quad (2.11)$$

Here \mathcal{T}_l includes quadrature points t_k condensed "near" zero, hence generating the long-range Gaussians (low-pass filters), and \mathcal{T}_s accumulates the increasing in $M \rightarrow \infty$ sequence of "large" sampling points t_k with the upper bound $C_0^2 \log^2(M)$, corresponding to the short-range Gaussians (high-pass filters). Notice that the quasi-optimal choice of the constant $C_0 \approx 3$ was determined in [7]. We further denote $\mathcal{K}_l := \{k | k = 0, 1, \dots, R_l\}$ and $\mathcal{K}_s := \{k | k = R_l + 1, \dots, M\}$.

Splitting (2.11) generates the additive decomposition of the canonical tensor \mathbf{P}_R onto the short- and long-range parts,

$$\mathbf{P}_R = \mathbf{P}_{R_s} + \mathbf{P}_{R_l},$$

where

$$\mathbf{P}_{R_s} = \sum_{t_k \in \mathcal{T}_s} \mathbf{p}_k^{(1)} \otimes \mathbf{p}_k^{(2)} \otimes \mathbf{p}_k^{(3)}, \quad \mathbf{P}_{R_l} = \sum_{t_k \in \mathcal{T}_l} \mathbf{p}_k^{(1)} \otimes \mathbf{p}_k^{(2)} \otimes \mathbf{p}_k^{(3)}. \quad (2.12)$$

The choice of the critical number $R_l = \#\mathcal{T}_l - 1$ (or equivalently, $R_s = \#\mathcal{T}_s = M - R_l$), that specifies the splitting $\mathcal{T} = \mathcal{T}_l \cup \mathcal{T}_s$, is determined by the *active support* of the short-range components such that one can cut off the functions $\mathbf{p}_k(x)$, $t_k \in \mathcal{T}_s$, outside of the sphere B_σ of radius $\sigma > 0$, subject to a certain threshold $\delta > 0$. For fixed $\delta > 0$, the choice of R_s is

uniquely defined by the (small) parameter σ and vice versa. The following two basic criteria, corresponding to (A) the max- and (B) L^1 -norms estimates can be applied given σ :

$$(A) \quad \mathcal{T}_s = \{t_k : a_k e^{-t_k^2 \sigma^2} \leq \delta\} \Leftrightarrow R_l = \min k : a_k e^{-t_k^2 \sigma^2} \leq \delta, \quad (2.13)$$

or

$$(B) \quad \mathcal{T}_s := \{t_k : a_k \int_{B_\sigma} e^{-t_k^2 x^2} dx \leq \delta\} \Leftrightarrow R_l = \min k : a_k \int_{B_\sigma} e^{-t_k^2 x^2} dx \leq \delta. \quad (2.14)$$

The quantitative estimates on the value of R_l can be easily calculated by using the explicit equation (2.7) for the quadrature parameters. For example, in case $C_0 = 3$ and $a(t) = 1$, criteria (A) implies that R_l solves the equation

$$\left(\frac{3R_l \log M}{M} \right)^2 \sigma^2 = \log\left(\frac{\mathfrak{h}_M}{\delta}\right).$$

Criteria (2.13) and (2.14) can be slightly modified depending on the particular applications to many-particles systems. For example, in electronic structure calculations, the parameter σ can be associated with the typical inter-atomic distance in the molecular system of interest.

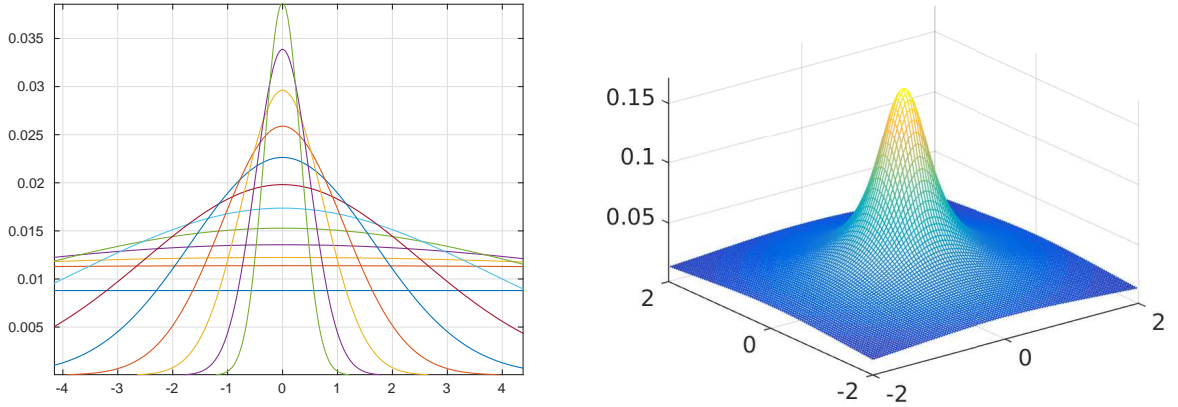


Figure 2.2: Long-range canonical vectors for $n = 1024$, $R = 20$, $R_l = 12$ and the corresponding potential.

Figures 2.2 and 2.3 illustrate the splitting (2.11) for the tensor \mathbf{P}_R computed on the $n \times n \times n$ grid with the parameters $R = 20$, $R_l = 12$ and $R_s = 8$, respectively. Figure 2.2 shows the long-range canonical vectors from \mathbf{P}_{R_l} in (2.12), while Figure 2.3 displays the short-range part described by \mathbf{P}_{R_s} . Following criteria (A) with $\delta \approx 10^{-4}$, the effective support for this splitting is determined by $\sigma = 0.9$. It can be seen that the complete Newton kernel depicted in Figure 2.1 covers the long-range behavior, while the function values of the tensor \mathbf{P}_{R_s} vanish exponentially fast apart of the effective support, as can be seen in Figure 2.3.

Inspection of the quadrature point distribution in (2.7) shows that the short- and long-range subsequences are nearly equally balanced distributed, so that one can expect approximately

$$R_s \approx R_l = M/2. \quad (2.15)$$

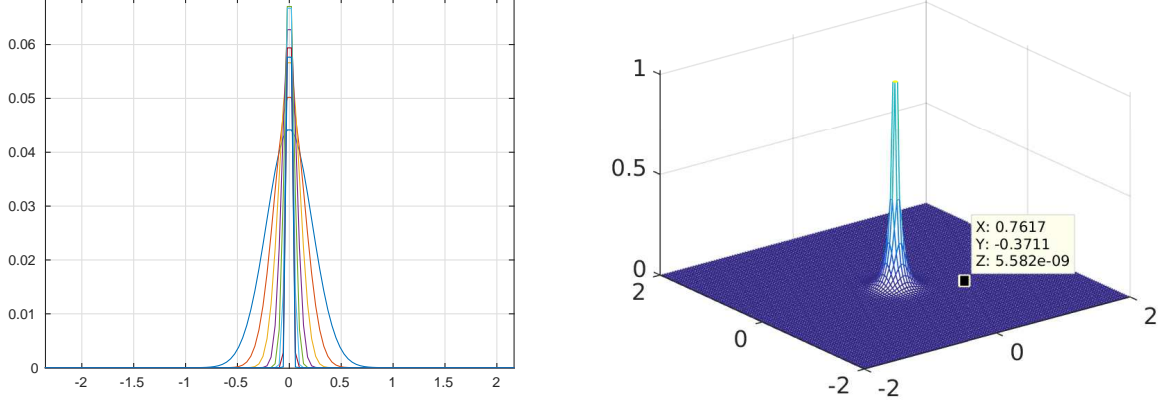


Figure 2.3: Short-range canonical vectors for $n = 1024$, $R = 20$, $R_s = 8$, and the corresponding potential.

The optimal choice may depend on the particular applications.

The advantage of the range separation in the splitting of the canonical tensor $\mathbf{P}_R \mapsto \mathbf{P}_{R_s} + \mathbf{P}_{R_l}$ in (2.12) is the opportunity for independent tensor representations of both sub-tensors \mathbf{P}_{R_s} and \mathbf{P}_{R_l} providing the separate treatment of the short- and long-range parts in the sum of many interaction potentials.

Finally, we notice that the *range separation principle* can be generalized to more than two-term splitting, taking into account the requirements of specific applications.

3 Tensor summation of range-separated potentials

In this section we describe how the range separated tensor representation of the generating potential function can be applied for the fast and accurate grid-based computation of a large sum of non-local potentials centered at arbitrary locations in the 3D volume. This is the bottleneck problem in numerical modeling of large N -particle systems.

3.1 Quasi-uniformly separable point distributions

One of the main limitations for the use of direct grid-based canonical/Tucker approximations to the large potential sums is due to the strong increase in tensor rank proportionally to the number of particles N in a system. Figure 3.1 shows the Tucker ranks for the protein-type system consisting of $N = 783$ atoms.

Given the generating kernel $p(\|x\|)$, we consider the problem of efficient calculating the weighted sum of a large number of single potentials located in a set \mathcal{S} of separable distributed points (sources), $x_\nu \in \mathbb{R}^3$, $\nu = 1, \dots, N$, embedded into the fixed bounding box $\Omega = [-b, b]^3$,

$$P_0(x) = \sum_{\nu=1}^N z_\nu p(\|x - x_\nu\|), \quad z_\nu \in \mathbb{R}. \quad (3.1)$$

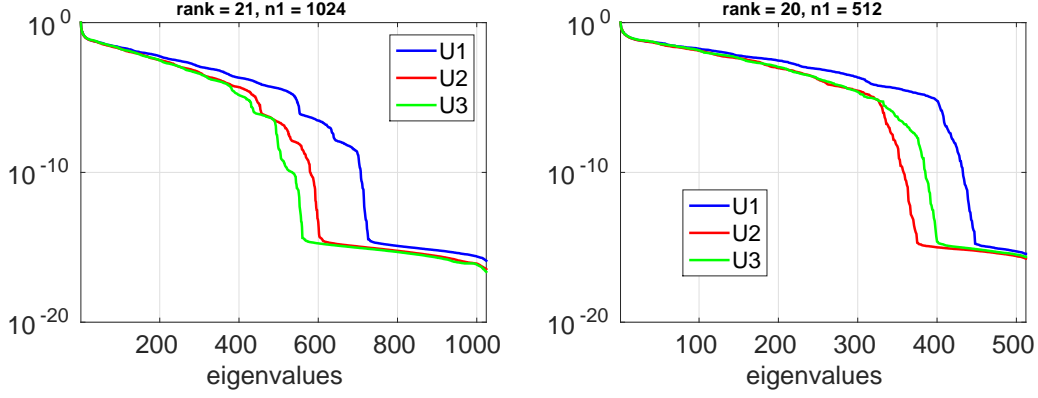


Figure 3.1: The directional Tucker ranks computed by RHOSVD for a protein-type system with $n=1024$ (left) and $n=512$ (right).

The function $p(\|x\|)$ is allowed to have slow polynomial decay in $1/\|x\|$ so that each individual source contributes essentially to the total potential at each point in Ω .

Definition 3.1 (*Well-separable point distribution*). Given a constant $\sigma_* > 0$, a set $\mathcal{S} = \{x_\nu\}$ of points in \mathbb{R}^d is called σ_* -separable if there holds

$$d(x_\nu, s_{\nu'}) := \|x_\nu - s_{\nu'}\| \geq \sigma_* \quad \text{for all } \nu \neq \nu'. \quad (3.2)$$

A family of point sets $\{\mathcal{S}_1, \dots, \mathcal{S}_m\}$, is called uniformly σ_* -separable if (3.2) holds for every set $\mathcal{S}_{m'}$, $m' = 1, 2, \dots, m$ independently of the number of particles in a set, $\#\mathcal{S}_{m'}$.

Condition (3.2) can be reformulated in terms of the so-called separation distance $q_{\mathcal{S}}$ of the point set \mathcal{S}

$$q_{\mathcal{S}} := \min_{s \in \mathcal{S}} \min_{x_\nu \in \mathcal{S} \setminus s} d(x_\nu, s) \geq \sigma_*. \quad (3.3)$$

Definition 3.1 on separability of point distributions is fulfilled, in particular, in the case of large molecular systems (proteins, crystals, polymers, nano-clusters), where all atomic centers are strictly separated from each other by a certain fixed *inter-atomic distance*. The same happens for lattice-type structures, where each atomic cluster within the unit cell is separated from the neighbors by a distance proportional to the lattice step-size.

Figure 3.2 (left) shows inter-particle distances in ascending order for a protein-type structure with 500 particles. The total number of distances equals to $N(N-1)/2$, where N is the number of particles. Figure 3.2 (right) indicates that the number of particles with small inter-particle distances is very moderate. In particular, for this example the number of pairs with interparticle distances less than 1\AA is about 0.04 % (≈ 110) of the total number of $2,495 \cdot 10^5$ distances.

In the following, for ease of presentation, we confine ourselves to the case of electrostatic potentials described by the Newton kernel $p(\|x\|) = \frac{1}{\|x\|}$.

3.2 Low-rank representation to the sum of long-range terms

First, we describe the tensor summation method for calculation of the collective potential of a multi-particle system that includes only the long-range contribution from the generating

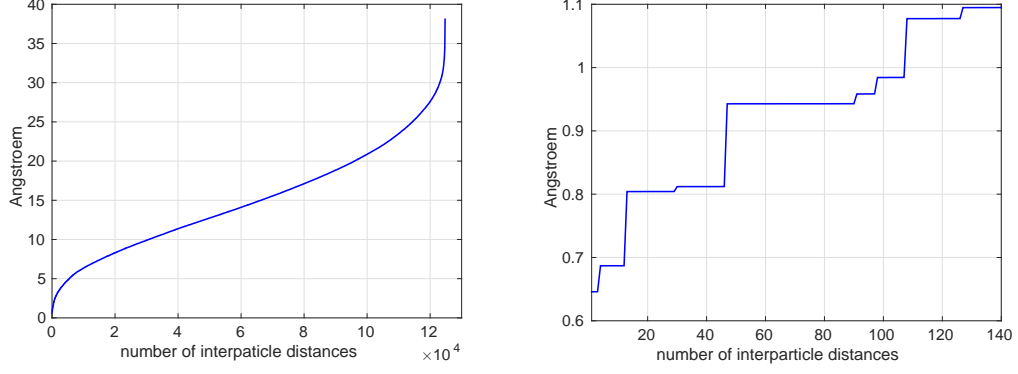


Figure 3.2: Inter-particle distances in a ascendant order for protein-type structure with 500 particles (left), zoom for the first 100 smallest inter-particle distances (right) .

kernel. We introduce the $n \times n \times n$ rectangular grid Ω_n in $\Omega = [-b, b]^3$, see §2.2, as well as the auxiliary $2n \times 2n \times 2n$ grid on the accompanying domain $\tilde{\Omega} = 2\Omega$ of double size. The canonical rank- R representation of the Newton kernel projected onto the $n \times n \times n$ grid is denoted by $\mathbf{P}_R \in \mathbb{R}^{n \times n \times n}$, see (2.10).

Consider the splitting (2.12) applied to the reference canonical tensor \mathbf{P}_R and to its accompanying version $\tilde{\mathbf{P}}_R = [\tilde{p}_R(i_1, i_2, i_3)]$, $i_\ell \in I_\ell$, $\ell = 1, 2, 3$, such that

$$\tilde{\mathbf{P}}_R = \tilde{\mathbf{P}}_{R_s} + \tilde{\mathbf{P}}_{R_l} \in \mathbb{R}^{2n \times 2n \times 2n}.$$

For technical reasons, we further assume that the tensor grid Ω_n is fine enough such that all charge centers $\mathcal{S} = \{x_\nu\}$ specifying the total electrostatic potential in (3.1) belong to the set of grid points, i.e., $x_\nu = (x_{\nu,1}, x_{\nu,2}, x_{\nu,3})^T = h(j_1^{(\nu)}, j_2^{(\nu)}, j_3^{(\nu)})^T \in \Omega_h$ with some indices $1 \leq j_1^{(i)}, j_2^{(i)}, j_3^{(i)} \leq n$.

The total electrostatic potential $P_0(x)$ in (3.1) is represented by a projected tensor $\mathbf{P}_0 \in \mathbb{R}^{n \times n \times n}$ that can be constructed by a direct sum of shift-and-windowing transforms of the reference tensor $\tilde{\mathbf{P}}_R$ (see [36] for more details),

$$\mathbf{P}_0 = \sum_{\nu=1}^N z_\nu \mathcal{W}_\nu(\tilde{\mathbf{P}}_R) = \sum_{\nu=1}^N z_\nu \mathcal{W}_\nu(\tilde{\mathbf{P}}_{R_s} + \tilde{\mathbf{P}}_{R_l}) =: \mathbf{P}_s + \mathbf{P}_l. \quad (3.4)$$

The shift-and-windowing transform \mathcal{W}_ν maps a reference tensor $\tilde{\mathbf{P}}_R \in \mathbb{R}^{2n \times 2n \times 2n}$ onto its sub-tensor of smaller size $n \times n \times n$, obtained by first shifting the center of the tensor $\tilde{\mathbf{P}}_R$ to the point x_ν and then tracing (windowing) the result onto the domain Ω_n :

$$\mathcal{W}_\nu : \tilde{\mathbf{P}}_R \mapsto \mathbf{P}^{(\nu)} = [p_{i_1, i_2, i_3}^{(\nu)}], \quad p_{i_1, i_2, i_3}^{(\nu)} := \tilde{p}_R(i_1 + j_1^{(\nu)}, i_2 + j_2^{(\nu)}, i_3 + j_3^{(\nu)}), \quad i_\ell \in I_\ell.$$

The point is that the Tucker rank of the full tensor sum \mathbf{P}_0 increases almost proportionally to the number N of particles in the system, see Figure 3.3, representing singular values of the side matrix in the canonical tensor \mathbf{P}_0 . On the other hand, the canonical rank of the tensor \mathbf{P}_0 shows up the pessimistic bound $\leq RN$.

To overcome this difficulty, in what follows, we consider the global tensor decomposition of only the "long-range part" in the tensor \mathbf{P}_0 , defined by

$$\mathbf{P}_l = \sum_{\nu=1}^N z_{\nu} \mathcal{W}_{\nu}(\tilde{\mathbf{P}}_{R_l}) = \sum_{\nu=1}^N z_{\nu} \mathcal{W}_{\nu} \left(\sum_{k \in \mathcal{K}_l} \tilde{\mathbf{p}}_k^{(1)} \otimes \tilde{\mathbf{p}}_k^{(2)} \otimes \tilde{\mathbf{p}}_k^{(3)} \right). \quad (3.5)$$

The initial canonical rank of the tensor \mathbf{P}_l equals to $R_l N$, and, again, it may increase dramatically for a large number of particles N . Since by construction the tensor \mathbf{P}_l approximates rather smooth function on the domain Ω , one may expect that the large initial rank can be reduced considerably to some value R_* that remains almost independent of N . The same beneficial property can be expected for the Tucker rank of \mathbf{P}_l . The principal ingredient of our tensor approach is the rank reduction in the initial canonical sum \mathbf{P}_l by application of the multigrid accelerated canonical-to-Tucker transform [42].

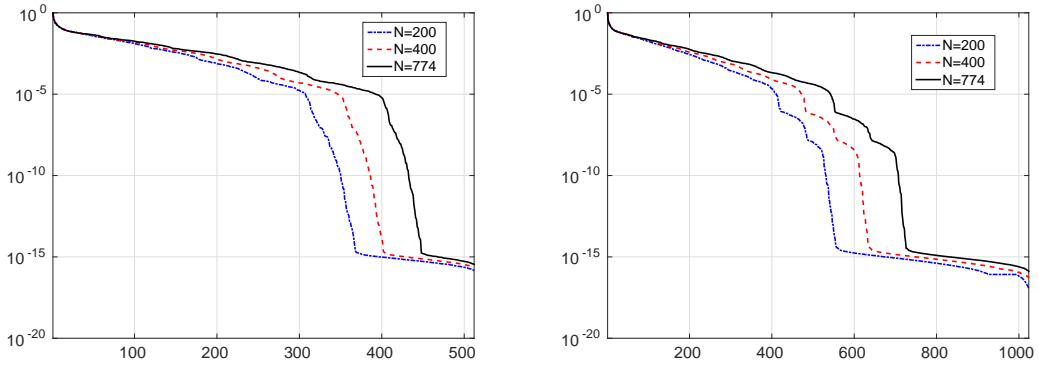


Figure 3.3: *Mode-1 singular values of the side matrix in the full potential sum vs. the number of particles $N = 200, 400, 774$ and grid-size n : $n = 512$ (left), $n = 1024$ (right).*

To simplify the exposition, we suppose that the tensor entries in \mathbf{P}_l are computed by collocation of Gaussian sums at the centers of the grid-cells. This provides the representation which is very close to that obtained by (2.10).

The following theorem proves the important result justifying the efficiency of range-separated formats applied to a class of radial basis functions $p(r)$: the Tucker ε -rank of the long-range part in accumulated sum of potentials computed in the bounding box $\Omega = [-b, b]^3$ remains almost uniformly bounded in the number of particles N (but depends on the size b of the domain).

Theorem 3.2 *Let the long-range part \mathbf{P}_l in the total interaction potential, see (3.5), correspond to the choice of splitting parameter in (2.15) with $M = O(\log^2 \varepsilon)$. Then the total ε -rank \mathbf{r}_0 of the Tucker approximation to the canonical tensor sum \mathbf{P}_l is bounded by*

$$|\mathbf{r}_0| := \text{rank}_{\text{Tuck}}(\mathbf{P}_l) = C b \log^{3/2}(|\log(\varepsilon/N)|),$$

where the constant C does not depend on the number of particles N .

Proof. We consider the Gaussian in normalized form $G_p(x) = e^{-\frac{x^2}{2p^2}}$ so that the relation $e^{-t_k^2 x^2} = e^{-\frac{x^2}{2p_k^2}}$ holds, i.e. we set, see (2.7),

$$t_k = \frac{1}{\sqrt{2p_k}}, \quad \text{with } t_k = k\mathfrak{h}_M, \quad k = 0, 1, \dots, M,$$

where $\mathfrak{h}_M = C_0 \log M/M$. Now criterion (B) in (2.14) on the bound of the L^1 -norm reads

$$a_k \int_a^\infty e^{-\frac{x^2}{2p_k^2}} \leq \frac{\varepsilon}{2} < 1, \quad a_k = \mathfrak{h}_M.$$

Now, we sketch the proof to the following steps. (A) We represent all shifted Gaussian functions, contributing to the total sum, in the fixed set of basis functions by using truncated Fourier series. (B) We prove that, on the "long-range" index set $k \in \mathcal{T}_l$, the parameter p_k remains uniformly bounded in N from below, implying the uniform bound on the number of terms in the ε -truncated Fourier series. (C) The summation of functions presented in the fixed Fourier basis set does not enlarge the Tucker rank, but only effects the Tucker core. The dependence on size of computational domain b remains in the explicit form.

Specifically, let us consider the rank-1 term in the splitting (2.12) with maximal index $k \in \mathcal{T}_l$. Taking into account the asymptotic choice $M = \log^2 \varepsilon$, see (2.9), where $\varepsilon > 0$ is the accuracy of the sinc-quadrature, the relation (2.15) implies

$$\max_{k \in \mathcal{T}_l} t_k = R_l \mathfrak{h}_M = \frac{M}{2} C_0 \log(M)/M \approx \log(M) = 2 \log(|\log(\varepsilon)|). \quad (3.6)$$

Now we consider the Fourier transform of the univariate Gaussian on $[-b, b]$,

$$G_p(x) = e^{-\frac{x^2}{2p^2}} = \sum_{m=0}^M \alpha_m \cos\left(\frac{\pi m x}{b}\right) + \eta, \quad \text{with } |\eta| = \left| \sum_{m=M+1}^\infty \alpha_m \cos\left(\frac{\pi m x}{b}\right) \right| < \varepsilon,$$

where

$$\alpha_m = \frac{\int_{-b}^b e^{-\frac{x^2}{2p^2}} \cos\left(\frac{\pi m x}{b}\right) dx}{|C_m|^2}, \quad \text{with } |C_m|^2 = \int_{-b}^b \cos^2\left(\frac{\pi m x}{b}\right) dx = \begin{cases} 2b, & \text{if } m = 0, \\ b, & \text{otherwise.} \end{cases}$$

Following arguments in [22] one obtains

$$\alpha_m = \left(p e^{-\frac{\pi^2 m^2 p^2}{2a^2}} - \xi_m \right) / |C_m|^2, \quad \text{where } 0 < \xi_m < \varepsilon.$$

Truncation of the coefficients α_m at $m = m_0$ such that $\alpha_{m_0} \leq \varepsilon$, leads to the bound

$$m_0 \geq \frac{\sqrt{2} b}{\pi p} \log^{0.5} \left(\frac{p}{(1 + |C_M|^2) \varepsilon} \right) = \frac{\sqrt{2} b}{\pi p} \log^{0.5} \left(\frac{p}{1 + b \varepsilon} \right).$$

On the other hand (3.6) implies

$$1/p_k \leq c \log(|\log \varepsilon|), \quad k \in \mathcal{T}_l, \quad \text{i.e. } 1/p_{R_l} \approx \log(|\log \varepsilon|),$$

that ensures the estimate on m_0 ,

$$m_0 = O(b \log^{3/2}(|\log \varepsilon|)). \quad (3.7)$$

Now following [36], we represent the Fourier transform of the shifted Gaussians by

$$G_p(x - x_\nu) = \sum_{m=0}^M \alpha_m \cos\left(\frac{\pi m(x - x_\nu)}{b}\right) + \eta_\nu, \quad |\eta_\nu| < \varepsilon,$$

which requires only the double number of trigonometric terms compared with the single Gaussian analyzed above. To compensate the possible increase in $|\sum_\nu \eta_\nu|$, we refine $\varepsilon \mapsto \varepsilon/N$. These estimates also apply to all Gaussian functions presented in the long-range sum since for $k \in \mathcal{T}_l$ they have larger values of p_k than p_{R_l} . Indeed, in view of (2.15) the number of summands in the long-range part is of the order $R_l = M/2 = O(\log^2 \varepsilon)$. Combining these arguments with (3.7) proves the resulting estimate. ■

Figure 3.4 illustrates fast decay of the Fourier coefficients for the "long-range" discrete Gaussians sampled on n -point grid (left) and a slow decay of Fourier coefficients for the "short-range" Gaussians (right). In the latter case, almost all coefficients remain essential, resulting in the full rank decomposition. The grid size is chosen as $n = 1024$.

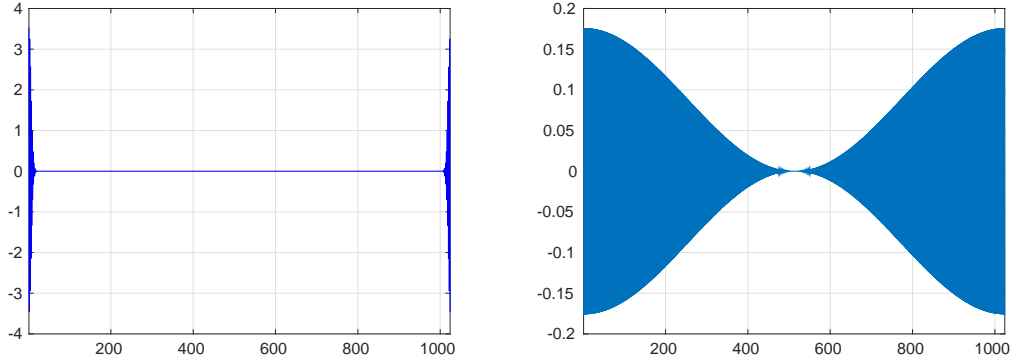


Figure 3.4: *Fourier coefficients of the long- (left) and short-range (right) discrete Gaussians.*

Remark 3.3 Notice that for fixed $\sigma > 0$ the σ -separability of the point distributions (see Definition 3.1) implies that the volume size of the computational box $[-b, b]^3$ should increase proportionally to the number of particles N , i.e., $b = O(N^{1/3})$. Hence, Theorem 3.2 indicates that since $r_l = O(b)$ the number of entries in the Tucker core of size $r_1 \times r_2 \times r_3$ can be estimated by CN . This asymptotic cost remains of the same order in N as that for the short-range part in the potential sum.

Figure 3.5, left, illustrates that the singular values of side matrices (i.e. bounds on the Tucker rank) for the long-range part (by choosing $R_l = 12$) exhibit fast exponential decay with a rate independent of the number of particles $N = 214, 405$, and 754 (cf. Figure 3.3). Figure 3.5, right, zooms into the first 50 singular values which are almost identical for the different values of N . The fast decay in these singular values guarantees the low-rank RHOSVD-based Tucker decomposition of the long-range part in the potential sum (see Appendix).

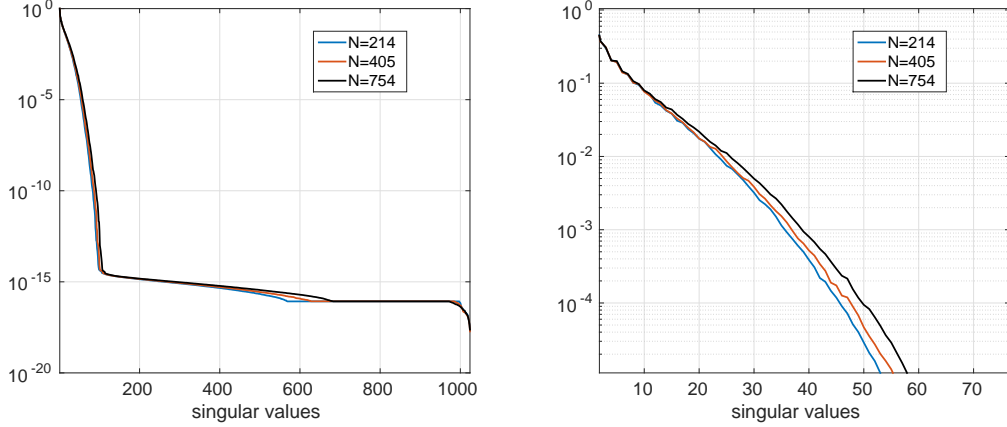


Figure 3.5: *Mode-1 singular values of side matrices for the long range part ($R_l = 12$) in the total potential vs. the number of particles N .*

	N	200	400	782	1728	4096
R_ℓ/R_s	Ranks full can.	4200	8400	16422	32288	86016
9/12	Ranks long range	1800	3600	7038	15552	36864
	RS-Tucker ranks	21,16,18	22,19,23	24,22,24	23,24,24	24,24,24
	RS-canonical rank	254	292	362	207	243
10/11	Ranks long range	2000	4000	7820	17280	40960
	RS-Tucker ranks	30,22,25	32,25,33	36,32,34	25,25,25	29,29,29
	RS-canonical rank	476	579	768	286	426

Table 3.1: *Tucker ranks and the RS canonical rank of the multiparticle potential sum versus the number of particles N for varying parameters R_ℓ and R_s for the grid size $n^3 = 1024^3$.*

Table 3.1 shows the Tucker ranks of sums of long-range ingredients in the electrostatic potentials for the N -particle clusters. The Newton kernel is generated on the grid with $n^3 = 1024^3$ in the computational box of size $b^3 = 40^3 \text{ \AA}$, with accuracy $\varepsilon = 10^{-4}$ and canonical rank 21. Particle clusters with 200, 400 and 782 atoms are taken as a part of protein-like multiparticle system. The clusters of size 1728 and 4096 correspond to the lattice structures of sizes $12 \times 12 \times 12$ and $16 \times 16 \times 16$, with randomly generated charges. The line “RS-canonical rank” shows the resulting rank after the canonical-to-Tucker and Tucker-to-canonical transform, with $\varepsilon_{C2T} = 4 \cdot 10^{-5}$ and $\varepsilon_{T2C} = 4 \cdot 10^{-6}$.

N/R_l	8	9	10	11	12	13
200	10,10,11	13,12,12	18,15,16	23,19,21	32,24,27	42,30,34
400	11,10,11	14,13,14	19,16,20	26,21,26	35,27,36	47,34,47
782	11,11,12	15,14,15	20,18,20	28,26,27	39,35,37	52,46,50

Table 3.2: *Tucker ranks $\mathbf{r} = (r_1, r_2, r_3)$ for the long-range parts of N -particle potentials.*

Table 3.2 represents the Tucker ranks $\mathbf{r} = (r_1, r_2, r_3)$ for the long-range parts of N -particle potentials. The reference Newton kernel is approximated on a 3D grid of size 2048^3 , with the rank $R = 29$ and with accuracy $\varepsilon_{\mathcal{N}} = 10^{-5}$. Here the Tucker tensor is computed with

the stopping criteria $\varepsilon_{T2C} = 10^{-5}$ in the ALS iteration. It can be seen that for fixed R_l the Tucker ranks increase very moderately in the system size N .

Fig. 3.6 demonstrates the decay in singular values of the side matrices (i.e., upper bound on the Tucker rank) in the canonical tensor representing potential sums of long-range parts for different $R_l = 10, 11$, and 12.

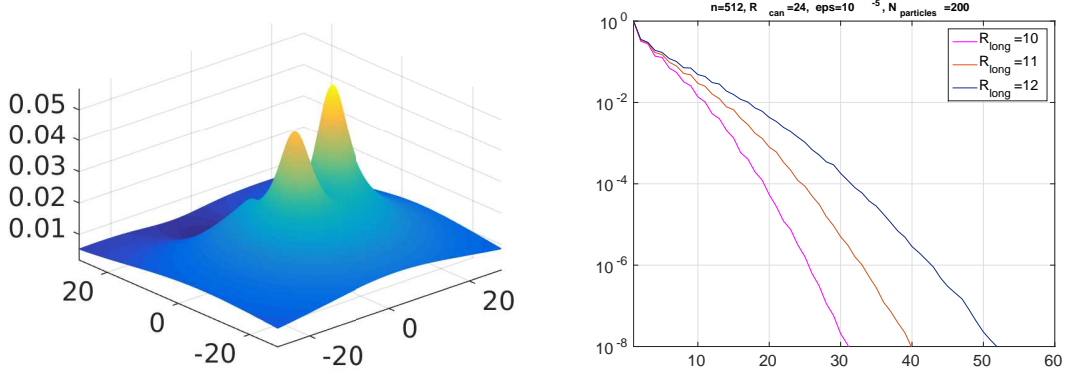


Figure 3.6: *Example of potential surface at level $z = 0$ (left) for a sum of $N_0 = 200$ particles computed using only their long-range parts with $R_l = 12$. Decay in singular values of the side matrices for the canonical tensor representing sums of long-range parts for $R_l = 10, 11$, and 12.*

The proof of Theorem 3.2 indicates that the Tucker directional vectors, living on large $n^{\otimes d}$ spatial grids, are represented in the uniform Fourier basis with a small number of terms. Hence, following the arguments in [22] and [36], we are able to apply the low-rank QTT tensor approximation [40] to these long vectors (see [52] for the case of matrices). The QTT tensor compression makes it possible to reduce the representation complexity of the long-range part in an RS tensor to the logarithmic scale in the univariate grid size, $O(\log n)$. This topic will be addressed in a forthcoming paper.

3.3 Range-separated canonical and Tucker tensor formats

We recall that the general canonical tensor is specified by a R -term sum of arbitrary rank-1 tensors as in (2.1), which makes it difficult to perform approximation process and multilinear algebra in such tensor format for large values of R . In applications to many-particle modeling the initial rank parameter R is proportional to the (large) number of particles N with pre-factor about 30, while the weights z_k can be rather arbitrary².

The idea on how to get rid of the "curse of ranks", that is the critical bottleneck in application of tensor methods to the problems like (3.1), is suggested by results in Theorem 3.2 on the almost uniform bound (in the number of particles N) of the Tucker rank for the long-range part in a multi-particle potential. Thanks to this beneficial property, we are able to introduce the new range-separated (RS) tensor formats based on the aggregated composition

² Notice that the sub-class of the so-called *orthogonal canonical tensors* [43] allows stable rank reduction, but suffers from the poor approximation capacity. Another class of "monotone" tensors providing stable canonical representation is specified by all positive canonical vectors, see [42, 38] for definition, which is the case in decomposition of the elliptic Green's kernels. Both classes of tensors do not suite problems like (3.1).

of the global low-rank canonical/Tucker tensor and the locally supported canonical tensors living on non-intersecting index sub-sets embedded into the large corporate multi-index set $\mathcal{I} = I_1 \times \dots \times I_d$, $I_\ell = \{1, \dots, n\}$. Such a parametrization attempts to represent the large multi-dimensional arrays with a storage cost linearly proportional to the number of cumulated inclusions (sub-tensors).

The structure of the *range-separated canonical/Tucker tensor formats* is specified by a combination of the local-global low parametric representations, which provide good approximation features in application to the problems of grid-based representation to many-particle interaction potentials with multiple singularities.

The following Definition 3.4 introduces the description of a sum of short range potentials having the local (up to some threshold) non-intersecting supports.

Definition 3.4 (*Cumulated canonical tensors*). Given the index set \mathcal{I} , a set of multi-indices (sources) $\mathcal{J} = \{\mathbf{j}^{(\nu)} := (j_1^{(\nu)}, j_2^{(\nu)}, \dots, j_d^{(\nu)})\}$, $\nu = 1, \dots, N$, $j_\ell^{(\nu)} \in I_\ell$, and the width index parameter $\gamma \in \mathbb{N}$ such that the γ -vicinity of each point $\mathbf{j}^{(\nu)} \in \mathcal{J}$, i.e. $\mathcal{J}_\gamma^{(\nu)} := \{\mathbf{j} : |\mathbf{j} - \mathbf{j}^{(\nu)}| \leq \gamma\}$ does not intersect all others

$$\mathcal{J}_\gamma^{(\nu)} \cap \mathcal{J}_\gamma^{(\nu')} = \emptyset, \quad \nu \neq \nu'.$$

A rank- R_0 cumulated canonical tensor \mathbf{U} , associated with \mathcal{J} and width parameter γ , is defined as a set of tensors which can be represented in form

$$\mathbf{U} = \sum_{\nu=1}^N c_\nu \mathbf{U}_\nu, \quad \text{with} \quad \text{rank}(\mathbf{U}_\nu) \leq R_0, \quad (3.8)$$

where the rank- R_0 canonical tensors $\mathbf{U}_\nu = [u_{\mathbf{j}}]$ are vanishing beyond the γ -vicinity of $\mathbf{j}^{(\nu)}$,

$$u_{\mathbf{j}} = 0 \quad \text{for} \quad \mathbf{j} \in \mathcal{I} \setminus \mathcal{J}_\gamma^{(\nu)}, \quad \nu = 1, \dots, N. \quad (3.9)$$

Given the particular point distribution, the effective support of the localized sub-tensors should be of the size close to the parameter σ_* , appearing in Def. 3.1, that introduces the σ_* -separable point distributions characterized by the separation parameter $\sigma_* > 0$. In this case, we use the relation $\sigma_* \approx \gamma h$, where $h = 2b/n$ is the mesh size of the computational $(n \times \dots \times n)$ -grid.

Figure 3.7 (left) illustrates the effective supports of a cumulated canonical tensor in the non-overlapping case, while Figure 3.7 (right) presents the supports for first 11 short-range canonical vectors (selected from rank-24 reference canonical tensor \mathbf{P}_R), which allows to make a choice for the parameter γ in separation criteria.

The separation criteria in Def. 3.4 leads to rather "aggressive" strategy for selection of the short-range part \mathbf{P}_{R_s} in the reference canonical tensor \mathbf{P}_R at the benefit of easy implementation of the cumulated canonical tensor (non-overlapping case). However, in some cases this may lead to overestimation of the Tucker/canonical rank in the long-range tensor component. To relax the criteria in Def. 3.4, we propose the "soft" strategy that allows to include a few (i.e., $O(1)$ for large N) neighboring particles into the local vicinity $\mathcal{J}_\gamma^{(\nu)}$ of the source point x_ν , which can be achieved by increasing the overlap parameter $\gamma > 0$. This allows to control the bound on the rank parameter of the long-range tensor almost uniformly in the system size N .

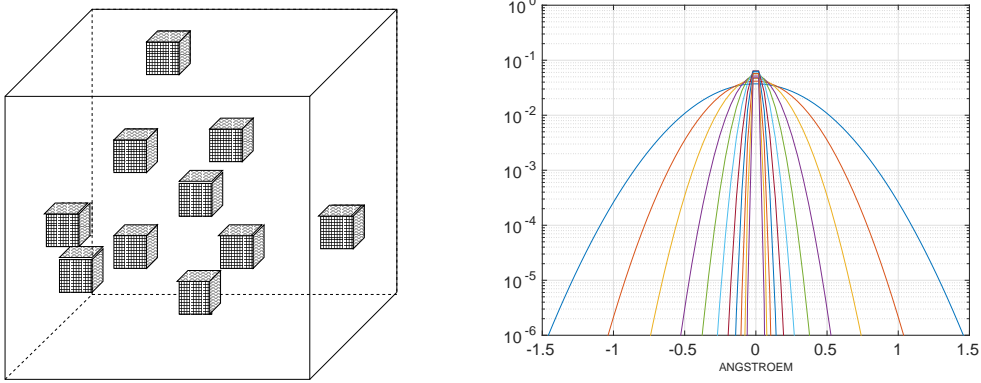


Figure 3.7: Schematic illustration of effective supports of the cumulated canonical tensor (left); Short-range canonical vectors for $k = 1, \dots, 11$, represented in logarithmic scale (right).

Example 3.5 For example, assume that the separation distance is equal to $\sigma_* = 0.8\text{\AA}$, corresponding to the example in Fig. 3.2, right, and the computational threshold is given $\varepsilon = 10^{-4}$. Then we find from Fig. 3.7 (right) that the "aggressive" criteria in Def. 3.4 leads to the choice $R_s = 10$, since the value of the canonical vector with $k = 11$ at point $x = \sigma_*$ is about 10^{-3} . Hence, in order to control the required rank parameter R_l , we have to extend the overlap area to larger parameter σ_* and, hence, to larger γ . This will lead to a small $O(1)$ -overlap between supports of the short range tensor components, but without asymptotic increase in the total complexity.

In the following, we distinguish a special subclass of *uniform CCT tensors*.

Definition 3.6 (Uniform CCT tensors). A CCT tensor in (3.8) is called *uniform* if all components \mathbf{U}_ν are generated by a single rank- R_0 tensor $\mathbf{U}_0 = \sum_{m=1}^{R_0} \mu_m \hat{\mathbf{u}}_m^{(1)} \otimes \dots \otimes \hat{\mathbf{u}}_m^{(d)}$, such that $\mathbf{U}_\nu|_{\mathcal{J}_\delta^{(\nu)}} = \mathbf{U}_0$.

Now we are in a position to define the range separated canonical and Tucker tensor formats in $\mathbb{R}^{n_1 \times \dots \times n_d}$. The range-separated canonical format is defined as follows.

Definition 3.7 (RS-canonical tensors).

The RS-canonical tensor format specifies the class of d -tensors $\mathbf{A} \in \mathbb{R}^{n_1 \times \dots \times n_d}$ which can be represented as a sum of a rank- R canonical tensor $\mathbf{U} \in \mathbb{R}^{n_1 \times \dots \times n_d}$ and a (uniform) cumulated canonical tensor generated by \mathbf{U}_0 with $\text{rank}(\mathbf{U}_0) \leq R_0$ as in Definition 3.6 (or more generally in Definition 3.4),

$$\mathbf{A} = \sum_{k=1}^R \xi_k \mathbf{u}_k^{(1)} \otimes \dots \otimes \mathbf{u}_k^{(d)} + \sum_{\nu=1}^N c_\nu \mathbf{U}_\nu, \quad (3.10)$$

where $\text{diam}(\text{supp} \mathbf{U}_\nu) \leq 2\gamma$ in the index size.

For a given grid-point $\mathbf{i} \in \mathcal{I} = I_1 \times \dots \times I_d$, we define the set of indices

$$\mathcal{L}(\mathbf{i}) := \{\nu \in \{1, \dots, N\} : \mathbf{i} \in \text{supp} \mathbf{U}_\nu\},$$

which label all short-range tensors \mathbf{U}_ν including the grid-point \mathbf{i} within its effective support.

Lemma 3.8 *The storage cost of RS-canonical tensor is estimated by*

$$\text{stor}(\mathbf{A}) \leq dRn + (d+1)N + dR_0\gamma.$$

Given $\mathbf{i} \in \mathcal{I}$, denote by $\bar{\mathbf{u}}_{i_\ell}^{(\ell)}$ the row-vector with index i_ℓ in the side matrix $U^{(\ell)} \in \mathbb{R}^{n_\ell \times R}$, and let $\xi = (\xi_1, \dots, \xi_d)$. Then the \mathbf{i} -th entry of the RS-canonical tensor $\mathbf{A} = [a_{\mathbf{i}}]$ can be calculated as a sum of long- and short-range contributions by

$$a_{\mathbf{i}} = \left(\odot_{\ell=1}^d \bar{\mathbf{u}}_{i_\ell}^{(\ell)} \right) \xi^T + \sum_{\nu \in \mathcal{L}(\mathbf{i})} c_\nu \mathbf{U}_\nu(\mathbf{i}),$$

at the expense $O(dR + 2d\gamma R_0)$.

Proof. Definition 3.7 implies that each RS-canonical tensor is uniquely defined by the following parametrization: rank- R canonical tensor \mathbf{U} , the rank- R_0 local reference canonical tensor \mathbf{U}_0 with mode-size bounded by 2γ , and list \mathcal{J} of the coordinates and weights of N particles. Hence the storage cost directly follows. To justify the representation complexity, we notice that by well-separability assumption (see Definition 3.1), we have $\#\mathcal{L}(\mathbf{i}) = O(1)$ for all $\mathbf{i} \in \mathcal{I}$. This proves the complexity bounds. \blacksquare

Now we define the class of RS-Tucker tensors.

Definition 3.9 (*RS-Tucker tensors*). The RS-Tucker tensor format specifies the class of d -tensors $\mathbf{A} \in \mathbb{R}^{n_1 \times \dots \times n_d}$ which can be represented as a sum of a rank- \mathbf{r} Tucker tensor \mathbf{V} and a (uniform) cumulated canonical tensor generated by \mathbf{U}_0 with $\text{rank}(\mathbf{U}_0) \leq R_0$ as in Definition 3.6 (or more generally in Definition 3.4),

$$\mathbf{A} = \boldsymbol{\beta} \times_1 V^{(1)} \times_2 V^{(2)} \dots \times_d V^{(d)} + \sum_{\nu=1}^N c_\nu \mathbf{U}_\nu, \quad (3.11)$$

where the tensor \mathbf{U}_ν , $\nu = 1, \dots, N$, has local support, i.e. $\text{diam}(\text{supp} \mathbf{U}_\nu) \leq 2\gamma$.

Similar to Lemma 3.8 the corresponding statement for the RS-Tucker tensors can be proven.

Lemma 3.10 *The storage size for RS-Tucker tensor does not exceed*

$$\text{stor}(\mathbf{A}) \leq r^d + drn + (d+1)N + dR_0\gamma.$$

Let the r_ℓ -vector $\mathbf{v}_{i_\ell}^{(\ell)}$ be the i_ℓ row of the matrix $V^{(\ell)}$. Then the \mathbf{i} -th element of the RS-Tucker tensor $\mathbf{A} = [a_{\mathbf{i}}]$ can be calculated by

$$a_{\mathbf{i}} = \boldsymbol{\beta} \times_1 \mathbf{v}_{i_1}^{(1)} \times_2 \mathbf{v}_{i_2}^{(2)} \dots \times_d \mathbf{v}_{i_d}^{(d)} + \sum_{\nu \in \mathcal{L}(\mathbf{i})} c_\nu \mathbf{U}_\nu(\mathbf{i})$$

at the expense $O(r^d + 2d\gamma R_0)$.

Proof. In view of Definition 3.9 each RS-Tucker tensor is uniquely defined by the following parametrization: the rank- $\mathbf{r} = (r_1, \dots, r_d)$ Tucker tensor $\mathbf{V} \in \mathbb{R}^{n_1 \times \dots \times n_d}$, the rank- R_0 local

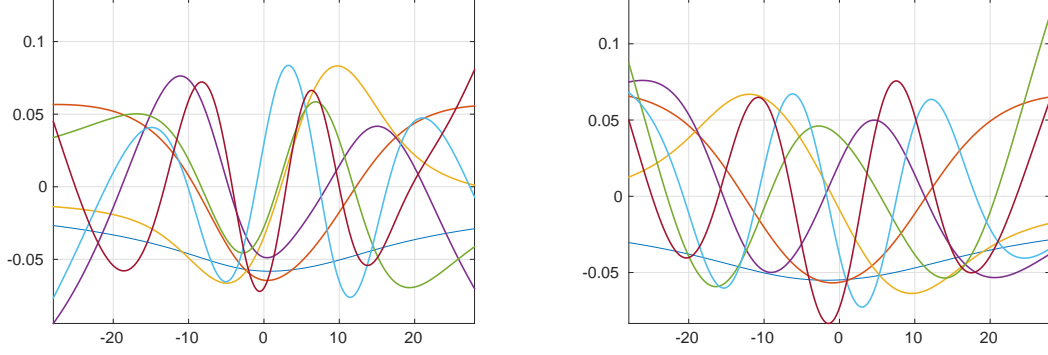


Figure 3.8: *Tucker vectors of the long range part in the RS tensor for 50 particles (left) and 500 particles (right).*

reference canonical tensor \mathbf{U}_0 with $\text{diam}(\text{supp}\mathbf{U}_0) \leq 2\gamma$, list \mathcal{J} of the coordinates of N centers of particles, $\{x_\nu\}$, and N weights $\{c_\nu\}$. This proves the complexity bounds. ■

Fig. 3.8 represents the first seven Tucker vectors of the long range part in the RS tensor for 50 and 500 particles. In both cases we observe the very smooth shape of the orthogonal functions which do not demonstrate the tendency to higher oscillations for larger number of particles.

The main computational benefits of the new range-separated canonical/Tucker tensor formats are explained by the important uniform bounds on the Tucker-rank of the long-range part in the large sum of interaction potentials (see Theorem 3.2 and numerics in §3.2). Moreover, we have the low storage cost for RS-canonical/Tucker tensors, cheap representation of each entry in an RS-tensor, possibility for simple implementation of multi-linear algebra on these tensors (see §3.4), which opens the opportunities for various applications.

The total rank of the sum of canonical tensors in \mathbf{U} , see (3.8), may become large for larger N since the pessimistic bound $\text{rank}(\mathbf{U}) \leq NR_0$. However, cumulated canonical tensors (CCT) have two beneficial features which are particularly useful in the low-rank tensor representation of large potential sums.

Proposition 3.11 (*Properties of CCT tensors*).

(A) *The local rank of a CCT tensor \mathbf{U} is bounded by R_0 :*

$$\text{rank}_{\text{loc}}(\mathbf{U}) := \max_{\nu} \text{rank}(\mathbf{U}_{\nu}) \leq R_0.$$

(B) *Local components in the CCT tensor (3.8) are “block orthogonal” in the sense*

$$\langle \mathbf{U}_{\nu}, \mathbf{U}_{\nu'} \rangle = 0, \quad \forall \nu \neq \nu'. \quad (3.12)$$

(C) *There holds $\|\mathbf{U}\| = \sum_{\nu=1}^N c_{\nu} \|\mathbf{U}_{\nu}\|$.*

Proof. Properties (A) and (B) simply follow by definition of CCT, while (C) is a direct consequence of (B). ■

If $R_0 = 1$, i.e. \mathbf{U} is the usual rank- N canonical tensor, then the property (B) in Proposition 3.11 leads to the definition of orthogonal canonical tensors in [43]; hence, in case $R_0 > 1$, we arrive at the generalization further called the *block orthogonal canonical tensors*.

The bound $R' = \text{rank}(\mathbf{U}) \leq NR_0$ indicates that the direct summation in (3.8) in the canonical/Tucker formats may lead to practically non-tractable representations. However, the block orthogonality property in Proposition 3.11, (B) allows to apply the stable RHOSVD approximation for the rank optimization, see Section 6. The stability of RHOSVD in the case of orthogonal canonical tensors was analyzed in [42, 38]. In what follows, we prove the stability of such tensor approximation applied to CCT representations.

Lemma 3.12 *Let the local canonical tensors be stable, i.e. $\sum_{m=1}^{R_0} \mu_m^2 \leq C \|\mathbf{U}_\nu\|^2$ (see Def. 3.6). Then the rank- \mathbf{r} RHOSVD-Tucker approximation $\mathbf{U}_{(\mathbf{r})}^0$ to the CCT, \mathbf{U} , provides the stable error bound*

$$\|\mathbf{U} - \mathbf{U}_{(\mathbf{r})}^0\| \leq C \sum_{\ell=1}^3 \left(\sum_{k=r_\ell+1}^{\min(n, R')} \sigma_{\ell, k}^2 \right)^{1/2} \|\mathbf{U}\|,$$

where $\sigma_{\ell, k}$ denote the singular values of the side matrices $U^{(\ell)}$, see (6.1).

Proof. We apply the general error estimate for RHOSVD approximation [42]

$$\|\mathbf{U} - \mathbf{U}_{(\mathbf{r})}^0\| \leq C \sum_{\ell=1}^3 \left(\sum_{k=r_\ell+1}^{\min(n, R')} \sigma_{\ell, k}^2 \right)^{1/2} \left(\sum_{\nu=1}^N \sum_{m=1}^{R_0} c_\nu^2 \mu_m^2 \right)^{1/2},$$

and then take into account the property (C), Proposition 3.11 to obtain

$$\sum_{\nu=1}^N \sum_{m=1}^{R_0} c_\nu^2 \mu_m^2 = \sum_{\nu=1}^N c_\nu^2 \sum_{m=1}^{R_0} \mu_m^2 \leq C \sum_{\nu=1}^N c_\nu^2 \|\mathbf{U}_\nu\|^2 = C \|\mathbf{U}\|^2,$$

which completes the proof. ■

We comment that the stability assumption in Lemma 3.12 is satisfied for the constructive canonical tensor approximation to the Newton and other types of Green's kernels obtained by sinc-quadrature based representations, where all skeleton vectors are non-negative and monotone.

Figures 3.9 show the accuracy of the RS-canonical tensor approximation to the electrostatic potential of a cluster of 400 particles at the middle section of the computational box $[-20, 20]^3 \text{ \AA}$, by using an $n \times n \times n$ 3D Cartesian grid with $n = 1024$, and step size $h = 0.04 \text{ \AA}$. The top-left figure shows the surface of the potential at the level $z = 0$, while the top-right figure shows the absolute error of the RS approximation with the ranks $R_l = 15$, $R_s = 11$, and the separation distance $\sigma^* = 1.5$. Bottom figures visualize the long-range (left) and short-range (right) parts of the RS-tensor, representing the potential sum.

Remark 3.13 *It is worth to note that in the case of higher dimensions, say, for $d > 3$, the local canonical tensors can be combined with the global tensor train (TT) format [53] such that the simple canonical-to-TT transform can be applied. In this case the RS-TT format can be introduced as a set of tensor represented as a sum of CCT term and the global TT-tensor. The complexity and structural analysis is completely similar to the case of RS-Canonical and RS-Tucker formats.*

We complete this section by the short outlook of algebraic operations on the RS tensors.

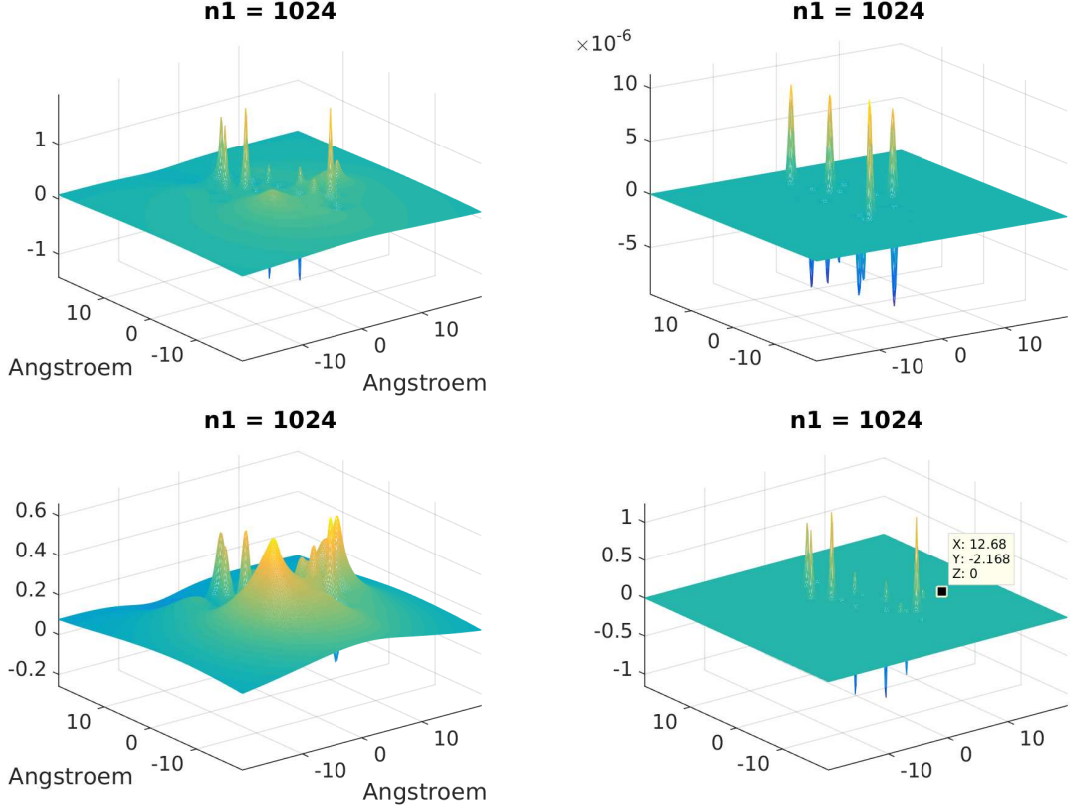


Figure 3.9: *Top: the electrostatic potential sum at a middle plane of a cluster with 400 atoms (left), and the error of the RS-canonical approximation (right). Bottom: long-range part of a sum (left), short range part of a sum (right).*

3.4 Algebraic operations on the RS canonical/Tucker tensors

Multilinear algebraic operations in the format of RS-canonical/Tucker tensor parametrization can be implemented by using 1D vector operations applied to both localized and global tensor components. In particular, the following operations on RS canonical/Tucker tensors can be realized efficiently: (a) storage of a tensor; (b) real space representation on a fine rectangular grid; (c) summation of many-particle interaction potentials represented on the fine tensor grid; (d) computation of scalar products; (e) computation of gradients and forces.

Estimates on the storage complexity for the RS-canonical and RS-Tucker formats were presented in Lemmas 3.8 and 3.10. Items (b) and (c) have been already addressed in the previous part. Calculation of the scalar product of two RS-canonical tensors in the form (3.10), defined on the same set \mathcal{S} of particle centers, can be reduced to the standard calculation of the cross scalar products between all elementary canonical tensors presented in (3.10). The numerical cost can be estimated by $O(\frac{1}{2}R(R-1)dn + 2\gamma RR_0N)$.

4 Sketch of possible applications

The RS tensor formats can be gainfully applied in computational problems including functions with multiple local singularities or cusps, Green kernels with essentially non-local behavior, as well as in various approximation problems treated by means of radial basis functions. In what follows, we present the brief explanations on how the RS tensor representations can be utilized to some computationally extensive problems: grid representation of multi-dimensional scattered data, interaction energy of charged many-particle system, computation of gradients and forces for many-particle potentials, construction of approximate boundary/interface conditions in the Poisson-Boltzmann equation describing the electrostatic potential of proteins. The detailed analysis of these examples will be the topic for forthcoming papers.

4.1 Multi-dimensional data modeling

In this section we briefly describe the model reduction approach to the problem of multi-dimensional data fitting based on the RS tensor approximation. The problems of multi-dimensional scattered data modeling and data mining are known to lead to computationally intensive simulations. We refer to [11, 33, 8, 24, 25, 30] concerning the discussion of most commonly used approaches for the approximating of multi-dimensional data and partial differential equations by using the radial basis functions.

The mathematical problems in scattered data modeling are concerned with the approximation of multi-variate function $f : \mathbb{R}^d \rightarrow \mathbb{R}$ ($d \geq 2$) by using samples given at a certain finite set $\mathcal{X} = \{x_1, \dots, x_N\} \subset \mathbb{R}^d$ of pairwise distinct points, see e.g. [11]. The function f may describe the surface of a solid body, the solution of a PDE, many-body potential field, multi-parametric characteristics of physical systems or some other multi-dimensional data.

In the particular problem setting one may be interested in recovering f from a given sampling vector $f|_{\mathcal{X}} = (f(x_1), \dots, f(x_N)) \in \mathbb{R}^N$. One of the traditional ways to tackle this problem is based on the construction of a suitable functional interpolant $P_N : \mathbb{R}^d \rightarrow \mathbb{R}$ satisfying $P_N|_{\mathcal{X}} = f|_{\mathcal{X}} =: \mathbf{f}$, i.e.,

$$P_N(x_j) = f(x_j), \quad \forall 1 \leq j \leq N, \quad (4.1)$$

or approximating the sampling vector $f|_{\mathcal{X}}$ on the set \mathcal{X} in the least squares sense. We consider the approach based on using *radial basis functions* providing the traditional tools for multivariate scattered data interpolation. To that end, the radial basis function (RBF) interpolation approach deals with a class of interpolants P_N in the form

$$P_N(x) = \sum_{j=1}^N c_j p(\|x - x_j\|) + Q(x), \quad Q \text{ is some smooth function}, \quad (4.2)$$

where $p : [0, \infty) \rightarrow \mathbb{R}$ is a fixed radial function, and $\|\cdot\|$ is the Euclidean norm on \mathbb{R}^d . To fix the idea, here we consider the particular version of (4.2) by setting $Q = 0$. Notice that the interpolation ansatz P_N in (4.2) has the same form as the multi-particle interaction potential in (3.1). This observation indicates that the numerical treatment of various problems based on the use of interpolant P_N can be handled by using the same tools of model reduction via rank-structured RS tensor approximation.

The particular choice of RBFs described in [11, 33] includes functions $p(r)$ in the form

$$r^\nu, \quad (1 + r^2)^\nu, \quad (\nu \in \mathbb{R}), \quad \exp(-r^2), \quad r^2 \log(r).$$

For our tensor based approach, the common feature of all these function classes is the existence of low-rank tensor approximations to the grid-based discretization of the RBF $p(\|x\|) = p(x_1, \dots, x_d)$, $x \in \mathbb{R}^d$, where we set $r = \|x\|$. We can extend the above examples by traditional functions commonly used in quantum chemistry, like Coulomb potential $1/r$, Slater function $\exp(-\lambda r)$, Yukawa potential $\exp(-\lambda r)/r$, as well as to the class of Matérn RBFs, traditionally applied in stochastic modeling [51]. Other examples are given by the Lennard-Jones (the Van der Waals) and dipole-dipole interaction potentials,

$$p(r) = 4\epsilon \left[\left(\frac{\sigma}{r} \right)^{12} - \left(\frac{\sigma}{r} \right)^6 \right], \quad \text{and} \quad p(r) = \frac{1}{r^3},$$

respectively, as well as by the Stokeslet [48], specified by the 3×3 matrix

$$p(\|x\|) = I/r + (xx^T)/r^3 \quad \text{for} \quad x \in \mathbb{R}^3.$$

In the context of numerical data modeling, we focus on the following computational tasks.

- (A) For fixed coefficient vector $\mathbf{c} = (c_1, \dots, c_N)^T \in \mathbb{R}^N$ find the efficient representation and storage of the interpolant in (4.2), sampled on fine tensor grid in $\Omega \subset \mathbb{R}^d$, that allows the $O(1)$ -fast point evaluation of P_N in the whole volume Ω and computation of various integral-differential operations on that interpolant like, gradients, forces, scalar products, convolution integrals, etc.
- (B) Finding the coefficient vector \mathbf{c} that solves the interpolation problem (4.1).

We look on the problems (A) and (B) with the intend to apply the RS tensor representation to the interpolant $P_N(x)$. The point is that the representation (4.2) can be viewed as the many-particle interaction potential (with charges c_j) considered in the previous sections. Hence, the RS tensor approximation can be successfully applied if the d -dimensional tensor approximating the RBF $p(\|x\|)$, $x \in \mathbb{R}^d$, on tensor grid, allows the low-rank canonical representation that can be split into the short- and long-range parts. This can be proven for functions listed above (see the example in §2.2 for the Newton kernel $1/\|x\|$). Notice that the Gaussian is already the rank-1 separable function.

Problem (A). To fix the idea, we consider the particular choice of the set $\mathcal{X} \subset \Omega := [0, 1]^d$, which can be represented by using the nearly optimal point sampling. The so-called optimal point sets realize the trade off between the separation distance $q_{\mathcal{X}} = \min_{s \in \mathcal{X}} \min_{x_\nu \in \mathcal{X} \setminus s} d(x_\nu, s)$, see (3.3), and the fill distance $h_{\mathcal{X}, \Omega} = \max_{y \in \Omega} d(\mathcal{X}, y)$, i.e. solve the problem, see [11],

$$q_{\mathcal{X}}/h_{\mathcal{X}, \Omega} \rightarrow \max.$$

We choose the set of points \mathcal{X} as a subset of the n^\otimes square grid Ω_h with the mesh-size $h = 1/(n-1)$, such that the separation distance satisfies $\sigma_* = q_{\mathcal{X}} \geq \alpha h$, $\alpha \geq 1$. Here $N \leq n^d$. The square grid Ω_h realizes an example of the almost optimal point set (see the discussion in [33]). The construction below also applies to nonuniform rectangular grids.

Now, we are in a position to apply the RS tensor representation to the total interpolant P_N . Let \mathbf{P}_R be the $n \times n \times n$ (say, for $d = 3$) rank- R tensor representing the RBF $p(\|\cdot\|)$ which allows the RS splitting by (2.12) generating the global RS representation (3.4). Then $P_N(x)$ can be represented by the tensor \mathbf{P}_N in the RS-Tucker (3.11) or RS-canonical (3.10) formats. The storage cost scales linear in both N and n , $O(N + dR_in)$. The tensor-based computation of different functionals on \mathbf{P}_N will be discussed in the following sections.

Problem (B). The interpolation problem (4.1) reduces to solve the linear system of equations for unknown coefficient vector $\mathbf{c} = (c_1, \dots, c_N)^T \in \mathbb{R}^N$,

$$A_{p,\mathcal{X}}\mathbf{c} = \mathbf{f}, \quad \text{where} \quad A_{p,\mathcal{X}} = [p(\|x_i - x_j\|)]_{1 \leq i,j \leq N} \in \mathbb{R}^{N \times N}, \quad (4.3)$$

with the symmetric matrix $A_{p,\mathcal{X}}$. Here, without loss of generality, we assume that the RBF, $p(\|\cdot\|)$, is continuous. The solvability conditions for the linear system (4.3) with the matrix $A_{p,\mathcal{X}}$ are discussed, for example, in [11]. We consider two principal cases.

Case (A). We assume that the point set \mathcal{X} coincides with the set of grid-points in Ω_h , i.e., $N = n^d$. Introducing the d -tuple multi-index $\mathbf{i} = (i_1, \dots, i_d)$ and $\mathbf{j} = (j_1, \dots, j_d)$, we reshape the matrix $A_{p,\mathcal{X}}$ into the tensor form

$$A_{p,\mathcal{X}} \mapsto \mathbf{A} = [a(i_1, j_1, \dots, i_d, j_d)] \in \bigotimes_{\ell=1}^d \mathbb{R}^{n \times n},$$

which corresponds to folding of an N -vector to a d -dimensional $n^{\otimes d}$ tensor. This d -level Toeplitz matrix is generated by the tensor \mathbf{P}_R obtained by collocation of the RBF $p(\|\cdot\|)$ on the grid Ω_h . Splitting the rank- R canonical tensor \mathbf{P}_R into a sum of short- and long-range terms,

$$\mathbf{P}_R = \mathbf{P}_{R_s} + \mathbf{P}_{R_l}, \quad \text{with} \quad \mathbf{P}_{R_l} = \sum_{k=1}^{R_l} \mathbf{p}_k^{(1)} \otimes \dots \otimes \mathbf{p}_k^{(d)},$$

allows to represent the matrix \mathbf{A} in the RS-canonical form as a sum of low-rank canonical tensors $\mathbf{A} = \mathbf{A}_{R_s} + \mathbf{A}_{R_l}$. Here, the first one corresponds to the diagonal (nearly diagonal in the case of "soft" separation strategy) matrix by assumption on the locality of \mathbf{P}_{R_s} . The second matrix takes the form of R_l -term Kronecker product sum

$$\mathbf{A}_{R_l} = \sum_{k=1}^{R_l} A_k^{(1)} \otimes \dots \otimes A_k^{(d)},$$

where each "univariate" matrix $A_k^{(\ell)} \in \mathbb{R}^{n \times n}$, $\ell = 1, \dots, d$, takes the symmetric Toeplitz form, generated by the first column vector $\mathbf{p}_k^{(\ell)}$. The storage complexity of the resultant RS representation to the matrix \mathbf{A} is estimated by $O(N + dR_l n)$. Similar matrix decompositions can be derived for the RS-Tucker and RS-TT representations of \mathbf{P}_R .

Now we represent the coefficient vector $\mathbf{c} \in \mathbb{R}^N$ as the d -dimensional $n^{\otimes d}$ tensor, $\mathbf{c} \mapsto \mathbf{C} \in \mathbb{R}^{n^{\otimes d}}$. Then the matrix vector multiplication $\mathbf{AC} = (\mathbf{A}_{R_s} + \mathbf{A}_{R_l})\mathbf{C}$ implemented in tensor format can be accomplished in $O(cN + dR_l N \log n)$ operations, i.e., with the asymptotically optimal cost in the number of sampling points N . The reason is that the matrix \mathbf{A}_{R_s} has the diagonal form, while the matrix-vector product between Toeplitz matrices $A_k^{(\ell)}$ constituting the Kronecker factors \mathbf{A}_{R_l} , and the corresponding n -columns (fibers) of the tensor \mathbf{C} , can be

implemented by 1D FFT in $O(n \log n)$ operations. One can customary enhance this scheme by introducing the low-rank tensor structure in the target vector (tensor) \mathbf{C} .

Case (B). This construction can be generalized to the situation when \mathcal{X} is a subset of Ω_h , i.e., $N < n^d$. In this case the complexity again scales linearly in N if $N = O(n^d)$. In the situation when $N \ll n^d$ the matrix-vector operation applies to the vector \mathbf{C} that vanishes beyond the small set \mathcal{X} . In this case the corresponding block-diagonal sub-matrices in $A_k^{(\ell)}$ loose the Toeplitz form thus resulting in the slight increase in the overall cost $O(N^{1+1/d})$.

In both cases (A) and (B) the presented new construction can be applied within any favorable preconditioned iteration for solving the linear system (4.3).

4.2 Interaction energy for charged many-particle system

Consider the calculation of the interaction energy (IE) for a charged multi-particle system. In the case of lattice-structured systems, the fast tensor-based computation scheme for IE was described in [37]. Recall that the interaction energy of the total electrostatic potential generated by the system of N charged particles located at $x_k \in \mathbb{R}^3$ ($k = 1, \dots, N$) is defined by the weighted sum

$$E_N = E_N(x_1, \dots, x_N) = \frac{1}{2} \sum_{j=1}^N z_j \sum_{k=1, k \neq j}^N \frac{z_k}{\|x_j - x_k\|}, \quad (4.4)$$

where z_k denotes the particle charge. Letting $\sigma > 0$ be the minimal physical distance between the centers of particles, we arrive at the σ -separable systems in the sense of Definition 3.1. The double sum in (4.4) applies only to the particle positions $\|x_j - x_k\| \geq \sigma$, hence, the quantity in (4.4) is computable also for singular kernels like $p(r) = 1/r$.

We observe that the quantity of interest E_N can be recast in terms of the interconnection matrix $A_{p,\mathcal{X}}$ defined by (4.3) with $p(r) = 1/r$, $\mathcal{X} = \{x_1, \dots, x_N\}$,

$$E_N = \frac{1}{2} \langle (A_{p,\mathcal{X}} - \text{diag} A_{p,\mathcal{X}}) \mathbf{z}, \mathbf{z} \rangle, \quad \text{where } \mathbf{z} = (z_1, \dots, z_N)^T. \quad (4.5)$$

Hence, E_N can be calculated by using the approach briefly addressed in the previous section.

Here, we describe this scheme in the more detail. Recall that the reference canonical tensor \mathbf{P}_R approximating the single Newton kernel on an $n \times n \times n$ tensor grid Ω_h in the computational box $\Omega = [-b, b]^3$ is represented by (2.10), where $h > 0$ is the fine mesh size. For ease of exposition, we assume that the particle centers x_k are located exactly at some grid points in Ω_h (otherwise, an additional approximation error may be introduced) such that each point x_k inherits some multi-index $\mathbf{i}_k \in \mathcal{I}$, and the origin $x = 0$ corresponds to the central point on the grid, $\mathbf{n}_0 = (n/2, n/2, n/2)$. In turn, the canonical tensor \mathbf{P}_0 approximating the total interaction potential $P_N(x)$ ($x \in \Omega$) for the N -particle system,

$$P_N(x) = \sum_{k=1}^N \frac{z_k}{\|x - x_k\|} \rightsquigarrow \mathbf{P}_0 = \mathbf{P}_s + \mathbf{P}_l \in \mathbb{R}^{n \times n \times n},$$

is represented by (3.4) as a sum of short- and long-range tensor components. Now the tensor $\mathbf{P}_0 = \mathbf{P}_0(x^h)$ is defined at each point $x^h \in \Omega_h$, and, in particular, in the vicinity

of each particle center x_k , i.e. at the grid-points $x_k + h\mathbf{e}$, where the directional vector $\mathbf{e} = (e_1, e_2, e_3)^T$ is specified by some choice of coordinates $e_\ell \in \{-1, 0, 1\}$ for $\ell = 1, 2, 3$. This allows to introduce the useful notations $\mathbf{P}_0(x_k + h\mathbf{e})$ which can be applied to all tensors leaving on Ω_h . Such notations simplify the definitions of entities like energy, gradients, forces, etc. applied to the RS tensors.

The following lemma describes the tensor scheme for calculating E_N by utilizing the long-range part \mathbf{P}_l only in the tensor representation of $P_N(x)$.

Lemma 4.1 *Let the effective support of the short-range components in the reference potential \mathbf{P}_R do not exceed $\sigma > 0$. Then the interaction energy E_N of the N -particle system can be calculated by using only the long range part in the total potential sum*

$$E_N = E_N(x_1, \dots, x_N) = \frac{1}{2} \sum_{j=1}^N z_j (\mathbf{P}_l(x_j) - z_j \mathbf{P}_{R_l}(x=0)), \quad (4.6)$$

in $O(dR_l N)$ operations, where R_l is the canonical rank of the long-range component.

Proof. Similar to [37], where the case of lattice structured systems was analyzed, we show that the interior sum in (4.4) can be obtained from the tensor \mathbf{P}_0 traced onto the centers of particles x_k , where the term corresponding to $x_j = x_k$ is removed,

$$\sum_{k=1, k \neq j}^N \frac{z_k}{\|x_j - x_k\|} \rightsquigarrow \mathbf{P}_0(x_j) - z_j \mathbf{P}_R(x=0).$$

Here the value of the reference canonical tensor \mathbf{P}_R , see (2.10), is evaluated at the origin $x=0$, i.e., corresponding to the multi-index $\mathbf{n}_0 = (n/2, n/2, n/2)$. Hence, we arrive at the tensor approximation

$$E_N \rightsquigarrow \frac{1}{2} \sum_{j=1}^N z_j (\mathbf{P}_0(x_j) - z_j \mathbf{P}_R(x=0)). \quad (4.7)$$

Now we split \mathbf{P}_0 into the long-range part (3.5) and the remaining short-range potential, to obtain $\mathbf{P}_0(x_j) = \mathbf{P}_s(x_j) + \mathbf{P}_l(x_j)$, and the same for the reference tensor \mathbf{P}_R . By assumption, the short-range part $\mathbf{P}_s(x_j)$ at point x_j in (4.7) consists only of the local term $P_{R_s}(x=0) = z_j \mathbf{P}_R(x=0)$. Due to the corresponding cancellations in the right-hand side of (4.7), we find that E_N depends only on \mathbf{P}_l , leading to the final tensor representation in (4.6).

We arrive at the linear complexity scaling $O(dR_l N)$ taking into account the $O(dR_l)$ cost of the point evaluation for the canonical tensor \mathbf{P}_l . ■

Table 4.1 shows the error of energy computation by (4.7) using the tensor summation with full rank canonical tensors. We use the data for protein type molecular system provided by the authors of [47]. This table indicates that the relative error of tensor computation remains of the order of 10^{-4} for the considered range of grid-size and the number molecular clusters. The canonical ranks R of the reference kernel are given by 34, 37, and 39 for $n \times n \times n$ grids with n equal to 4096, 8192 and 16384, respectively. CPU times for energy computation with these sizes of molecular clusters are small for both tensor and the straightforward calculation schemes. Tensor computation on the grid of size $n^3 = 8192^3$ takes $8 \cdot 10^{-4}$ s, while using the original formula (4.4) it amounts to 0.04s.

3D Grid, mesh size	N	100	200	400	782
	Exact E_N	-8.4888	-18.1712	-35.9625	-90.2027
$4096^3, 1.37 \cdot 10^{-2}$	$E_N - E_{N,T}$	0.01	$2 \cdot 10^{-5}$	0.0034	0.0084
	$(E_N - E_{N,T})/E_N$	0.0012	10^{-5}	10^{-4}	$3 \cdot 10^{-4}$
$8192^3, 6.8 \cdot 10^{-3}$	$E_N - E_{N,T}$	0.0028	0.005	0.0074	0.0245
	$(E_N - E_{N,T})/E_N$	$3 \cdot 10^{-4}$	$3 \cdot 10^{-4}$	$2 \cdot 10^{-4}$	$3 \cdot 10^{-4}$
$16384^3, 3.4 \cdot 10^{-3}$	$E_N - E_{N,T}$	0.0021	0.0013	0.0039	0.0053
	$(E_N - E_{N,T})/E_N$	$2 \cdot 10^{-4}$	10^{-4}	10^{-4}	10^{-4}

Table 4.1: Absolute and relative errors in the interaction energy of N -particle clusters computed by full canonical tensor approximation ($R_s = 0$).

Table 4.2 presents the error of energy computation by (4.7) by using the RS tensor format with $R_l = 14$ and $R_s = 13$. Remarkably, that the approximation error does not exceed the errors in Table 4.1.

3D Grid, mesh size	N	100	200	400	782
	Exact E_N	-8.4888	-18.1712	-35.9625	-90.2027
$4096^3, 1.37 \cdot 10^{-2}$	$E_N - E_{N,T}$	0.0044	0.0191	0.0265	0.1254
	$(E_N - E_{N,T})/E_N$	0.0005	0.0002	0.0007	0.0014
$8192^3, 6.8 \cdot 10^{-3}$	$E_N - E_{N,T}$	0.0010	0.0044	0.0074	0.0064
	$(E_N - E_{N,T})/E_N$	10^{-4}	$2 \cdot 10^{-4}$	$2 \cdot 10^{-4}$	10^{-4}
$16384^3, 3.4 \cdot 10^{-3}$	$E_N - E_{N,T}$	0.0015	0.0010	0.002	0.0001
	$(E_N - E_{N,T})/E_N$	$2 \cdot 10^{-4}$	10^{-4}	10^{-4}	10^{-5}

Table 4.2: Absolute and relative errors in the interaction energy of N -particle clusters computed by RS-tensor approximation with $R_l = 14$, ($R_s = 13$).

Table 4.3 represents the approximation error in E_N computed by RS tensor representation (4.6) for the different values of system size. Grid size is $n^3 = 4096^3$, $h = 0.0137$, canonical rank for the reference tensor is $R = 29$. The short range part of the RS tensor is taken as $R_s = 10$.

N	200	300	400	500	600	700
Exact E_N	-17.91	-26.47	-35.56	-47.1009	-62.32	-77.47
$E_N - E_{N,T}$	0.0018	0.0004	0.0026	0.0083	0.019	0.017
$(E_N - E_{N,T})/E_N$	$6 \cdot 10^{-5}$	$9 \cdot 10^{-7}$	$3.8 \cdot 10^{-5}$	$2.4 \cdot 10^{-4}$	$3.0 \cdot 10^{-4}$	$2.0 \cdot 10^{-4}$

Table 4.3: Error in the interaction energy of clusters of N particles computed by the RS tensor approach ($R_s = 10$).

Table 4.4 shows the results for several clusters of particles generated by random assignment of charges z_j to finite lattices of size 8^3 , 12^3 , $16 \times 16 \times 8$ and 16^3 . Newton kernel is approximated with $\varepsilon_N = 10^{-4}$ on the grid of size $n^3 = 4096^3$, $h = 0.0137$, with the rank $R = 25$. Computation of the interaction energy was performed using the only long-range part with $R_l = 12$. For the rank reduction the multigrid C2T algorithm is used [42], with the

rank truncation parameters $\varepsilon_{C2T} = 10^{-5}$, $\varepsilon_{T2C} = 10^{-6}$. The box size is about $40 \times 40 \times 40$ atomic units, with the mesh size $h = 0.0098$.

N of particles	512	1728	2048	4096
Exact E_N	51.8439	-133.9060	-138.5562	-207.8477
$E_N - E_{N,T}$	0.1145	0.1317	0.2263	0.2174
$(E_N - E_{N,T})/E_N$	0.0022	0.001	0.0016	0.001
Ranks full can.	12800	43200	51200	102400
Tucker ranks	31, 29, 30	43,42,43	51, 51, 33	53,54,54
Reduced RS rank	688	1248	1256	1740
Time stand. Sum.	0.011	0.12	0.18	0.79
Time Tens Sum.	$2 \cdot 10^{-5}$	$6 \cdot 10^{-5}$	$7 \cdot 10^{-5}$	$1.5 \cdot 10^{-4}$

Table 4.4: *Errors in the interaction energy of N -particle clusters computed by RS tensor approximation with the long-range rank parameter $R_l = 12$ ($R_s = 13$).*

Table 4.4 illustrates that the relative accuracy of energy calculations by using the RS tensor format remains of the order of 10^{-3} almost independent of the cluster size. Tucker ranks only slightly increase with the system size N . The computation time for the tensor \mathbf{P}_l remains almost constant, while the point evaluations time for this tensor (with pre-computed data) increases linearly in N , see Lemma 4.1.

4.3 Gradients and forces

Calculation of electrostatic forces and gradients of the interaction potentials in multiparticle systems is a computationally extensive problem. The algorithms based on Ewald summation technique were discussed in [20, 31]. We propose an alternative approach using the RS tensor format.

First, we consider computation of gradients. Given an RS-canonical tensor \mathbf{A} as in (3.10) with the width parameter $\gamma > 0$, the discrete gradient $\nabla_h = (\nabla_1, \dots, \nabla_d)^T$ applied to the long-range part in \mathbf{A} at all grid points of Ω_h simultaneously, can be calculated as the R -term canonical tensor by applying the simple one-dimensional finite-difference (FD) operations to the long-range part in $\mathbf{A} = \mathbf{A}_s + \mathbf{A}_l$,

$$\nabla_h \mathbf{A}_l = \sum_{k=1}^R \xi_k (\mathbf{G}_k^{(1)}, \dots, \mathbf{G}_k^{(d)})^T, \quad (4.8)$$

with tensor entries

$$\mathbf{G}_k^{(\ell)} = \mathbf{u}_k^{(1)} \otimes \dots \otimes \nabla_\ell \mathbf{u}_k^{(\ell)} \otimes \dots \otimes \mathbf{u}_k^{(d)},$$

where ∇_ℓ ($\ell = 1, \dots, d$) is the univariate FD differentiation scheme (by using backward or central differences). Numerical complexity of the representation (4.8) can be estimated by $O(dRn)$ provided that the canonical rank is almost uniformly bounded in the number of particles. The gradient operator applies locally to each short-range term in (3.10) which amounts in the complexity $O(dR_0\gamma N)$.

The gradient of an RS-Tucker tensor, for example, for evaluation of the field

$$\mathbf{F}(x) = -\nabla P(x) = \sum_{k=1, k \neq j}^N z_k \frac{x - x_k}{\|x - x_k\|^3},$$

can be calculated in a similar way. Furthermore, in the setting of §4.2, the force vector \mathbf{F}_j on the particle j is obtained by differentiating the electrostatic potential energy $E_N(x_1, \dots, x_N)$ with respect to x_j ,

$$\mathbf{F}_j = -\frac{\partial}{\partial x_j} E_N = -\nabla_{|x_j} E_N,$$

which can be calculated explicitly (see [31]) in the form,

$$\mathbf{F}_j = \frac{1}{2} z_j \sum_{k=1, k \neq j}^N z_k \frac{x_j - x_k}{\|x_j - x_k\|^3}.$$

The Ewald summation technique for force calculations was presented in [20, 31]. In principle, it is possible to construct the RS tensor representation for this vector field directly by using the radial basis function $p(r) = 1/r^2$.

Here we describe the alternative approach based on numerical differentiation of the energy functional by using RS tensor representation of the N -particle interaction potential on fine spacial grid. The differentiation in RS-tensor format with respect to x_j is based on the explicit representation (4.6), which can be rewritten in the form

$$E_N(x_1, \dots, x_N) = \hat{E}_N(x_1, \dots, x_N) - \frac{1}{2} \left(\sum_{j=1}^N z_j^2 \right) \mathbf{P}_{R_l}(x=0), \quad (4.9)$$

where $\hat{E}_N(x_1, \dots, x_N) = \frac{1}{2} \sum_{j=1}^N z_j \mathbf{P}_l(x_j)$ denotes the "non-calibrated" interaction energy with the long-range tensor component \mathbf{P}_l . In the following discussion, for definiteness, we set $j = N$. Since the second term in (4.9) does not depend on the particle positions it can be omitted in calculation of variations in E_N with respect to x_N . Hence we arrive at the representation for the first difference in direction \mathbf{e}_i , $i = 1, 2, 3$,

$$E_N(x_1, \dots, x_N) - E_N(x_1, \dots, x_N - h\mathbf{e}_i) = \hat{E}_N(x_1, \dots, x_N) - \hat{E}_N(x_1, \dots, x_N - h\mathbf{e}_i).$$

The straightforward implementation of the above relation for three different values of $\mathbf{e}_1 = (1, 0, 0)^T$, $\mathbf{e}_2 = (0, 1, 0)^T$ and $\mathbf{e}_3 = (0, 0, 1)^T$ is reduced to four calls of the basic procedure for computation of the tensor \mathbf{P}_l corresponding to *four* different dispositions of points x_1, \dots, x_N leading to the cost $O(dRn)$.

However, the factor *four* can be reduced to merely one taking into account that the two canonical/Tucker tensors \mathbf{P}_l computed for particle positions $(x_1, \dots, x_{N-1}, x_N)$ and $(x_1, \dots, x_{N-1}, x_N - h\mathbf{e}_i)$ differ in a small part (since positions x_1, \dots, x_{N-1} remain fixed). This requires only minor modifications compared with the repeating the full calculation of $\hat{E}_N(x_1, \dots, x_N)$.

4.4 Regularization scheme for the Poisson-Boltzmann equation

We describe the application scheme to the Poisson-Boltzmann equation (PBE) commonly used for numerical modeling of the electrostatic potential of proteins. The traditional numerical approaches to PBE are based on either multigrid [50] or domain decomposition [13] methods.

Consider a solvated biomolecular system modeled by dielectrically separated domains with singular Coulomb potentials distributed in the molecular region. For schematic representation, we consider the system occupying a rectangular domain Ω with boundary $\partial\Omega$, see Fig. 4.1. The solute (molecule) region is represented by Ω_m and the solvent region by Ω_s .

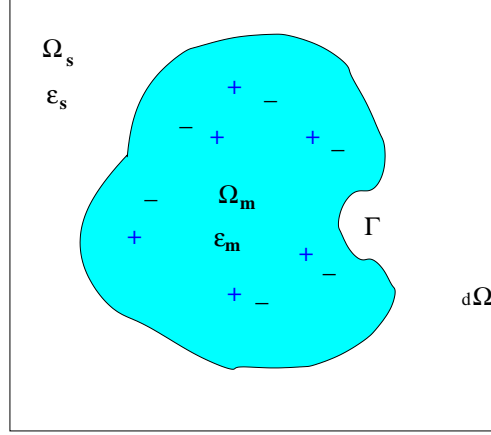


Figure 4.1: Computational domain for PBE.

The linearized Poisson-Boltzmann equation takes a form, see [50],

$$-\nabla \cdot (\epsilon \nabla u) + \kappa^2 u = \rho_f \quad \text{in } \Omega, \quad (4.10)$$

where u denotes the target electrostatic potential of a protein, and $\rho_f = \sum_{k=1}^N z_k \delta(\|x - x_k\|)$ is the scaled singular charge distribution supported at points x_k in Ω_m , where δ is the Dirac delta. Here $\epsilon = 1$ and $\kappa = 0$ in Ω_m , while in the solvent region Ω_s we have $\kappa \geq 0$ and $\epsilon \leq 1$. The boundary conditions on the external boundary $\partial\Omega$ can be specified depending on the particular problem setting. For definiteness, we impose the simplest Dirichlet boundary condition $u|_{\partial\Omega} = 0$. The interface conditions on the interior boundary $\Gamma = \partial\Omega_m$ arise from the dielectric theory:

$$[u] = 0, \quad \left[\epsilon \frac{\partial u}{\partial n} \right] \quad \text{on } \Gamma. \quad (4.11)$$

The practically useful solution methods for the PBE are based on regularization schemes aiming at removing the singular component from the potentials in the governing equation. Among others, we consider one of the most commonly used approaches based on the additive splitting of the potential only in the molecular region Ω_m , see [50]. To that end we introduce the additive splitting

$$u = u^r + u^s, \quad \text{where } u^s = 0 \quad \text{in } \Omega_s,$$

and where the singular component satisfies the equation

$$-\epsilon_m \Delta u^s = \rho_f \quad \text{in } \Omega_m; \quad u^s = 0 \quad \text{on } \Gamma. \quad (4.12)$$

Now equation (4.10) can be transformed to that for the regular potential u^r :

$$-\nabla \cdot (\epsilon \nabla u^r) + \kappa^2 u^r = \rho_f \quad \text{in } \Omega, \quad (4.13)$$

$$[u^r] = 0, \quad \left[\epsilon \frac{\partial u^r}{\partial n} \right] = -\epsilon_m \frac{\partial u^s}{\partial n}, \quad \text{on } \Gamma.$$

To facilitate the solution of equation (4.12) with singular data we define the singular potential U in the free space by

$$\epsilon_m \Delta U = \rho_f \quad \text{in } \mathbb{R}^3,$$

and introduce its restriction U^s onto Ω_m ,

$$U^s = U|_{\overline{\Omega}_m} \quad \text{in } \overline{\Omega}_m; \quad U^s = 0 \quad \text{in } \Omega_s.$$

Then we have $u^s = U^s + u^h$, where a harmonic function u^h compensates the discontinuity of U^s on Γ ,

$$\Delta u^h = 0 \quad \text{in } \Omega_m; \quad u^h = -U^s \quad \text{on } \Gamma.$$

The advantage of this formulation is due to (a) the absence of singularities in the solution u^r , and (b) the localization of the solution splitting only on the domain Ω_m . Calculating the singular potential U which may include a sum of hundreds or even thousands of single Newton kernels in 3D leads to a challenging computational problem. In our approach it can be represented on large tensor grids with controlled precision by using the range separated tensor formats described above. The long-range component in the formatted parametrization remains smooth and allows global low-rank representation. The approach can be combined with the reduced model approach for PBE with the parametric coefficients [47].

It is worth noting that the short-range part in the tensor representation of U does not contribute to the right-hand side in the interface conditions on Γ in equation (4.13). This crucial simplification is possible since the physical distance between the atomic centers in protein modeling is bounded from below by the fixed constant $\sigma > 0$, while the effective support of the localized parts in the tensor representation of U can be chosen as the half of σ . Moreover, all normal derivatives can be easily calculated by differentiation of univariate canonical vectors in the long-range part of the electrostatic potential U precomputed on a fine tensor grid in \mathbb{R}^3 (see §4.3). Hence, the numerical cost to build up the interface conditions in (4.13) becomes negligible compared with the solution of the equation (4.13). We conclude with the following

Proposition 4.2 *Let the effective support of the short-range components in the reference potential \mathbf{P}_R be chosen not larger than $\sigma/2$. Then the interface conditions in the regularized formulation (4.13) of the PBE depend only on the low-rank long-range component in the free-space electrostatic potential of the system. The numerical cost to build up the interface conditions on Γ in (4.13) does not depend on the number of particles N .*

Finally, we notice the important characterization of the protein molecule given by the electrostatic solvation energy [50], which is the difference between the electrostatic free energy in the solvated state (described by the PBE) and the electrostatic free energy in the absence of solvent, i.e. E_N . Now the electrostatic solvation energy can be computed in the framework of the new regularized formulation (4.13) of PBE.

5 Conclusions

In this paper, we introduce and analyze the new range-separated canonical and Tucker tensor formats for the grid representation of the long-range interaction potentials in multiparticle systems. One can distinguish the RS tensors from the conventional rank-structured representations due to their intrinsic features, originating from tensor approximation to multivariate functions with multiple singularities, in particular, generated by a weighted sum of the classical Green’s kernels.

We show that the tensor approximation to the particle interaction potentials allows to split their long- and short-range parts providing their efficient representation and numerical treatment in the low-rank RS tensor formats. Indeed, the long-range part in the potential sum can be represented on a grid by the low-rank canonical/Tucker tensor globally in the computational box, while its short-range component is parametrized by a reference tensor of local support and a list of particle coordinates and charges. In particular, we prove that the Tucker rank of the long-range part in N -particle potential depends only logarithmically on the number of particles in the system.

The RS formats prove to be well suited for summation of the electrostatic potentials in large many-particle systems in a box (e.g. proteins or large molecular clusters), providing the low-parametric tensor representation of the total potential at any point of the fine 3D $n \times n \times n$ Cartesian grid. For the computer realization of the RS tensor decomposition, a canonical-to-Tucker rank reduction algorithm is applied resulting in the $O(n \log N)$ grid representation of the long-range part in the many-particle potential. Notice that the existing approaches are limited by the $O(n^3)$ complexity contrary to the almost linear scaling in univariate mesh size n for the RS tensor format.

Numerical tests confirm the theoretical rank estimates and the asymptotically optimal complexity bound $O(N)$. In particular, the electrostatic potential for N -particle systems (up to several thousands of atoms) is computed in Matlab with controllable accuracy, resulting in the RS tensor living on large 3D grids of size up to $n^3 = 10^{12}$.

As examples of possible applications, we describe the tensor based representation to the electrostatic free energy of a protein in the absence of solvent and illustrate the efficiency by numerical tests. We observe that for moderate accuracy requirements, the application of the RS canonical/Tucker formats exhibits very mild limitations on the system size. This situation may occur in the problems of protein docking and classification of biomolecules. Furthermore, we demonstrate how the RS tensor decomposition allows to easily compute the gradients and forces for multi-particle interaction potentials. The benefits of the RS tensors in multi-dimensional scattered data modeling are also discussed. Finally, we propose the enhanced regularized formulation for the Poisson-Boltzmann equation that is based on pre-computing of only the long-range part in the electrostatic potential of protein in free space \mathbb{R}^3 .

The presented analysis of the RS tensor formats indicates their potential benefits in various applications related to modeling of many particle systems, and addresses a number of new interesting theoretical and algorithmic questions on rank-structured tensor approximation of multivariate functions with generally located point singularities.

Finally, we notice that the RS tensor approach can be easily extended to the case of multi-dimensional scattered data in \mathbb{R}^d for $d > 3$.

6 Appendix: CP-to-Tucker tensor transform by reduced HOSVD

For the reader's convenience, in this section we recall the main ingredients of the rank-reduction approach for canonical tensors with large initial rank. The multigrid accelerated canonical-to-Tucker tensor transform combined with the Tucker-to-canonical scheme was invented in [42] for the rank optimization of 3D function related canonical tensors given as the large sum of rank-1 components. It was proved to be a useful approach to many problems arising in grid-based computations in quantum chemistry.

The approximation results in [28, 39] indicate that the tensor representation of regular multidimensional functions with point singularities can lead to their accurate low-rank decomposition. However, to compute the Tucker (or canonical) decomposition in a traditional way as described in [16], requires information on all entries of a tensor. The so-called higher-order SVD (HOSVD) method [16] amounts to $O(n^{d+1})$ operations and memory cost.

The numerical complexity can be reduced dramatically if the initial tensor is given in the canonical format, presumably with rather large rank parameter R . In general, it might be storage/time consuming to generate, first, a full tensor from the canonical one, and then apply the HOSVD based Tucker decomposition to it. The canonical-to-Tucker decomposition eliminates this step, and turns the Tucker decomposition into the alternating least square (ALS) problem with easily precomputed initial orthogonal Tucker subspaces.

Specifically, the canonical-to-Tucker decomposition eliminates finding the initial guess for the standard Tucker ALS iteration (see [16, 44]) by using the SVD of the side matrices in the canonical tensor representation. This approach, called the reduced HOSVD (RHOSVD), was introduced in [35, 42]. The multigrid version of the RHOSVD allows to reduce the dominating cost in 3D case to $O(Rn)$ [34].

Without loss of generality, we consider the case $d = 3$. To define the reduced rank- \mathbf{r} HOSVD type Tucker approximation to the tensor in (2.1), we set $n_\ell = n$ and suppose for definiteness that $n \leq R$. Now the SVD of the side-matrix $U^{(\ell)}$ is given by

$$U^{(\ell)} = Z^{(\ell)} D_\ell V^{(\ell)T} = \sum_{k=1}^n \sigma_{\ell,k} \mathbf{z}_k^{(\ell)} \mathbf{v}_k^{(\ell)T}, \quad \mathbf{z}_k^{(\ell)} \in \mathbb{R}^n, \quad \mathbf{v}_k^{(\ell)} \in \mathbb{R}^R, \quad (6.1)$$

with the orthogonal matrices $Z^{(\ell)} = [\mathbf{z}_1^{(\ell)}, \dots, \mathbf{z}_n^{(\ell)}]$, and $V^{(\ell)} = [\mathbf{v}_1^{(\ell)}, \dots, \mathbf{v}_n^{(\ell)}]$, $\ell = 1, 2, 3$. Given the rank parameter $\mathbf{r} = (r_1, r_2, r_3)$ with $r_1, r_2, r_3 < n$, we introduce the truncated SVD of the side-matrix

$$U^{(\ell)} \mapsto U_0^{(\ell)} = \sum_{k=1}^{r_\ell} \sigma_{\ell,k} \mathbf{z}_k^{(\ell)} \mathbf{v}_k^{(\ell)T} = Z_0^{(\ell)} D_{\ell,0} V_0^{(\ell)T}, \quad \ell = 1, 2, 3,$$

where $D_{\ell,0} = \text{diag}\{\sigma_{\ell,1}, \sigma_{\ell,2}, \dots, \sigma_{\ell,r_\ell}\}$ and $Z_0^{(\ell)} \in \mathbb{R}^{n \times r_\ell}$, $V_0^{(\ell)} \in \mathbb{R}^{R \times r_\ell}$, represent the orthogonal factors being the respective sub-matrices in the SVD factors of $U^{(\ell)}$.

Definition 6.1 ([42]). *The RHOSVD approximation of \mathbf{U} in (2.4), further called $\mathbf{U}_{(\mathbf{r})}^0$, is defined as the rank- \mathbf{r} Tucker tensor obtained by the projection of \mathbf{U} onto the orthogonal matrices of the dominating singular vectors in $Z_0^{(\ell)} \in \mathbb{R}^{n \times r_\ell}$, ($\ell = 1, 2, 3$),*

$$\mathbf{U} \mapsto \mathbf{U}_{(\mathbf{r})}^0 = \boldsymbol{\xi} \times_1 U_0^{(1)} \times_2 U_0^{(2)} \times_d U_0^{(3)}. \quad (6.2)$$

For the ease of presentation, we further sketch the algorithm *Canonical-to-Tucker* for the 3D tensor. This includes the following basic steps:

Input data: Side matrices $U^{(\ell)} = [\mathbf{u}_1^{(\ell)} \dots \mathbf{u}_R^{(\ell)}] \in \mathbb{R}^{n_\ell \times R}$, $\ell = 1, 2, 3$, composed of the vectors $\mathbf{u}_k^{(\ell)} \in \mathbb{R}^{n_\ell}$, $k = 1, \dots, R$, see (2.1); maximal Tucker-rank parameter \mathbf{r} ; maximal number of the ALS iterations m_{max} (usually a small number).

(I) Compute the singular value decomposition (SVD) of the side matrices:

$$U^{(\ell)} = Z^{(\ell)} D^{(\ell)} V^{(\ell)}, \quad \ell = 1, 2, 3.$$

Discard the singular vectors in $Z^{(\ell)}$ and the respective singular values up to given rank threshold, yielding the small orthogonal matrices $Z_0^{(\ell)} \in \mathbb{R}^{n_\ell \times r_\ell}$, and diagonal matrices $D_{\ell,0} \in \mathbb{R}^{r_\ell \times r_\ell}$, $\ell = 1, 2, 3$.

(II) Project the side matrices $U^{(\ell)}$ onto the orthogonal basis set defined by $Z_0^{(\ell)}$

$$U^{(\ell)} \mapsto \tilde{U}^{(\ell)} = (Z_0^{(\ell)})^T U^{(\ell)} = D_{\ell,0} V_0^{(\ell)T}, \quad \tilde{U}^{(\ell)} \in \mathbb{R}^{r_\ell \times R}, \quad \ell = 1, 2, 3. \quad (6.3)$$

and compute $\mathbf{U}_{(\mathbf{r})}^0$ as in (6.2).

(III) (Find dominating subspaces). Implement the following ALS iteration (IV) m_{max} times at most, starting from the RHOSVD initial guess $\mathbf{U}_{(\mathbf{r})}^0$.

(IV) Perform ALS iteration for $\ell = 1, 2, 3$:

◊ For $\ell = 1$: construct the partially projected image of the full tensor,

$$\mathbf{U} \mapsto \tilde{\mathbf{U}}_1 = \sum_{k=1}^R c_k \mathbf{u}_k^{(1)} \otimes \tilde{\mathbf{u}}_k^{(2)} \otimes \tilde{\mathbf{u}}_k^{(3)}, \quad c_k \in \mathbb{R}. \quad (6.4)$$

Here $\mathbf{u}_k^{(1)} \in \mathbb{R}^{n_1}$ is in physical space for mode $\ell = 1$, while $\tilde{\mathbf{u}}_k^{(2)} \in \mathbb{R}^{r_2}$ and $\tilde{\mathbf{u}}_k^{(3)} \in \mathbb{R}^{r_3}$, the column vectors of $\tilde{U}^{(2)}$ and $\tilde{U}^{(3)}$, respectively, leave the small coefficients index sets.

◊ Reshape the tensor $\tilde{\mathbf{U}}_1 \in \mathbb{R}^{n_1 \times r_2 \times r_3}$ into a matrix $M_{U_1} \in \mathbb{R}^{n_1 \times (r_2 r_3)}$, representing the span of the optimized subset of mode-1 columns of the partially projected tensor $\tilde{\mathbf{U}}_1$. Compute the SVD of the matrix M_{U_1} :

$$M_{U_1} = Z^{(1)} S^{(1)} V^{(1)},$$

and truncate the set of singular vectors in $Z^{(1)} \mapsto \tilde{Z}^{(1)} \in \mathbb{R}^{n_1 \times r_1}$, according to the restriction on the mode-1 Tucker rank, r_1 .

◊ Update the current approximation to the mode-1 dominating subspace, $Z_{r_1}^{(1)} \mapsto \tilde{Z}^{(1)}$.

◊ Implement the single step of the ALS iteration for mode $\ell = 2$ and $\ell = 3$.

◊ End of the complete ALS iteration sweep.

◊ Repeat the complete ALS iteration m_{max} times to obtain the optimized Tucker orthogonal side matrices $\tilde{Z}^{(1)}$, $\tilde{Z}^{(2)}$, $\tilde{Z}^{(3)}$, and final projected image $\tilde{\mathbf{U}}_3$.

(V) Project the final iterated tensor $\tilde{\mathbf{U}}_3$ in (6.4) using the resultant basis set in $\tilde{Z}^{(3)}$ to obtain the core tensor, $\boldsymbol{\beta} \in \mathbb{R}^{r_1 \times r_2 \times r_3}$.

Output data: The Tucker core tensor $\boldsymbol{\beta}$ and the orthogonal side matrices $\tilde{Z}^{(\ell)}$, $\ell = 1, 2, 3$.

In such a way it is possible to obtain a Tucker decomposition of a canonical tensor with large mode-size and with rather large ranks, as it may be the case for biomolecules or the electron densities in electronic structure calculations. The multigrid version of the Canonical-to-Tucker algorithm allows to avoid the expensive SVD calculation in Step (I) thus reducing the cost of first two steps to $O(Rn)$.

The *Canonical-to-Tucker* algorithm can be easily modified to use an ε -truncation stopping criterion. Notice that the maximal canonical rank³ of the core tensor β does not exceed r^2 in the case of $r = r_\ell$, see [42, 34].

In our particular application we use the multigrid accelerated C2T algorithm, which eliminates the singular value decomposition of the side matrices $U^{(\ell)}$, $\ell = 1, 2, 3$ of size $n \times R$ having the cost $O(n^2 R)$ for $n < R$ or $O(R^2 n)$ for $n > R$ and thus reduces the numerical costs to $O(Rn)$ [42, 34].

References

- [1] T. Beck. Real-space mesh techniques in density-functional theory. *Rev. Mod. Phys.*, 72:1041–1080, 2000.
- [2] P. Benner, S. Dolgov, V. Khoromskaia, and B. N. Khoromskij. Fast iterative solution of the bethe-salpeter eigenvalue problem using low-rank and QTT tensor approximation. *arXiv:1602.02646*, 2016.
- [3] P. Benner, S. Dolgov, A. Onwunta, and M. Stoll. Low-rank solvers for unsteady Stokes-Brinkman optimal control problem with random data. *Comp. Meth. Appl. Mech. Eng.*, 304(1):2654, 2016.
- [4] P. Benner, S. Gugercin, and K. Willcox. A survey of projection-based model order reduction methods for parametrized dynamical systems. *SIAM Review*, 57:483–531, 2015.
- [5] P. Benner, V. Khoromskaia, and B. N. Khoromskij. A reduced basis approach for calculation of the Bethe-Salpeter excitation energies using low-rank tensor factorizations. *Mol. Physics*, 114(7-8):1148–1161, 2016.
- [6] P. Benner, V. L. Mehrmann, and D. C. Sorensen. *Dimension reduction of large-scale systems*, volume 45. Springer Verlag, 2005.
- [7] C. Bertoglio and B. N. Khoromskij. Low-rank quadrature-based tensor approximation of the Galerkin projected Newton/Yukawa kernels. *Comp. Phys. Comm.*, 183(4):904–912, 2012.
- [8] G. Beylkin, J. Garcke, and M. J. Mohlenkamp. Multivariate regression and machine learning with sums of separable functions. *SIAM J Sci. Comp.*, 31(3):1840–1857, 2009.
- [9] S. F. Boys, G. B. Cook, C. M. Reeves, and I. Shavitt. Automatic fundamental calculations of molecular structure. *Nature*, 178:1207–1209, 1956.
- [10] D. Braess. *Nonlinear approximation theory*. Springer-Verlag, 1986.
- [11] M. D. Buhmann. *Radial Basis Functions*. Cambridge University Press, 2003.
- [12] E. Cances, V. Ehrlacher, and T. Lelièvre. Greedy algorithms for high-dimensional eigenvalue problems. *J. Constr. Approx.*, 40:387–423, 2014.
- [13] E. Cances, Y. Maday, and B. Stamm. Domain decomposition for implicit solvation models. *J. Chem. Phys.*, 139:054111, 2013.
- [14] W. Dahmen, R. Devore, L. Grasedyck, and A. Süli. Tensor-sparsity of solutions to high-dimensional elliptic partial differential equations. *Found. Comput. Math.*, DOI 10.1007/s10208-015-9265-9:1–62, 2015.
- [15] T. Darden, D. York, and L. Pedersen. Particle mesh Ewald: An $O(N \log N)$ method for Ewald sums in large systems. *J. Chem. Phys.*, 98:10089–10091, 1993.
- [16] L. De Lathauwer, B. De Moor, and J. Vandewalle. A multilinear singular value decomposition. *SIAM J. Matrix Anal. Appl.*, 21:1253–1278, 2000.
- [17] H. De Sterck. An adaptive algebraic multigrid algorithm for low-rank canonical tensor decomposition. *SIAM J. Sci. Comput.*, 34:A1351–A1379, 2012.

³Further reduction of the canonical rank in the small-size core tensor β can be implemented by using the ALS-canonical iterative scheme, described e.g. in [44].

- [18] H. De Sterck and K. Miller. An adaptive algebraic multigrid algorithm for low-rank canonical tensor decomposition. *SIAM J. Sci. Comput.*, 35:B1–B24, 2013.
- [19] M. Deserno and C. Holm. How to mesh up Ewald sums. I. A theoretical and numerical comparison of various particle mesh routines. *J. Chem. Phys.*, 109(18):7678–7693, 1998.
- [20] M. Deserno and C. Holm. How to mesh up Ewald sums. II. A theoretical and numerical comparison of various particle mesh routines. *J. Chem. Phys.*, 109(18):7694–7701, 1998.
- [21] S. Dolgov, J. W. Pearson, D. Savostyanov, and M. Stoll. Fast tensor product solvers for optimization problems with fractional differential equations as constraints. *Appl. Math. Comp.*, 273:604–623, 2016.
- [22] S. V. Dolgov, B. N. Khoromskij, and I. V. Oseledets. Fast solution of multi-dimensional parabolic problems in the tensor train/quantized tensor train-format with initial application to the Fokker-Planck equation. *SIAM J. Sci. Comp.*, 34(6):A3016–A3038, 2012.
- [23] P. Ewald. Die berechnung optische und elektrostatischer gitterpotentiale. *Annalen der Physik*, 369(3):253–287, 1921.
- [24] B. Fornberg and N. Flyer. Solving PDEs with radial basis functions. *Acta Numerica*, 24:215–258, 2005.
- [25] B. Fornberg and N. Flyer. *A Primer on Radial Basis Functions with Applications to the Geosciences*. SIAM, 2015.
- [26] L. Grasedyck, D. Kressner, and C. Tobler. A literature survey of low-rank tensor approximation techniques. *arXiv:1302.7121v1*, 2013.
- [27] L. Greengard and V. Rokhlin. A fast algorithm for particle simulations. *J. Comp. Phys.*, 73:325, 1987.
- [28] W. Hackbusch and B. Khoromskij. Low-rank Kronecker product approximation to multi-dimensional nonlocal operators. part I. Separable approximation of multi-variate functions. *Computing*, 76:177–202, 2006.
- [29] W. Hackbusch and R. Schneider. Tensor spaces and hierarchical tensor representations. In: *Lecture Notes in Computer Science and Engineering*, S. Dahlke, W. Dahmen, et al. eds., Springer, pages 237–262, 2014.
- [30] J. S. Hesthaven, G. Rozza, and B. Stamm. *Certified Reduced Basis Methods for Parametrized Partial Differential Equations*. Springer, Berlin, 2016.
- [31] R. W. Hockney and J. W. Eastwood. *Computer Simulation Using Particles*. IOP, Bristol, 1988.
- [32] P. H. Hünenberger and J. A. McCammon. Effect of artificial periodicity in simulations of biomolecules under Ewald boundary conditions: a continuum electrostatics study. *Biophys. Chemistry*, 78:69–88, 1999.
- [33] A. Iske. *Multiresolution methods in scattered data modelling*. Springer, 2004.
- [34] V. Khoromskaia. *Numerical Solution of the Hartree-Fock Equation by Multilevel Tensor-structured methods*. PhD thesis, Technical University of Berlin, 2010.
- [35] V. Khoromskaia and B. N. Khoromskij. Low rank Tucker tensor approximation to the classical potentials. *Centr. Europ. J. Math.*, 5(3):1–28, 2007.
- [36] V. Khoromskaia and B. N. Khoromskij. Grid-based lattice summation of electrostatic potentials by assembled rank-structured tensor approximation. *Comp. Phys. Comm.*, 185(12), 2014.
- [37] V. Khoromskaia and B. N. Khoromskij. Tensor numerical methods in quantum chemistry: from Hartree-Fock to excitation energies. *Phys. Chem. Chem. Phys.*, 17:31491 – 31509, 2015.
- [38] V. Khoromskaia and B. N. Khoromskij. Fast tensor method for summation of long-range potentials on 3D lattices with defects. *Numer. Lin. Alg. Appl.*, 23:249–271, 2016.
- [39] B. N. Khoromskij. Structured rank- (r_1, \dots, r_d) decomposition of function-related operators in \mathbb{R}^d . *Comp. Meth. Appl. Math*, 6(2):194–220, 2006.

- [40] B. N. Khoromskij. $O(d \log N)$ -quantics approximation of N - d tensors in high-dimensional numerical modeling. *J. Constr. Approx.*, 34(2):257–289, 2011.
- [41] B. N. Khoromskij. Tensors-structured numerical methods in scientific computing: Survey on recent advances. *Chemometr. Intell. Lab. Syst.*, 110:1–19, 2012.
- [42] B. N. Khoromskij and V. Khoromskaia. Multigrid accelerated tensor approximation of function related multidimensional arrays. *SIAM J. Sci. Comp.*, 31(4):3002–3026, 2009.
- [43] T. Kolda. Orthogonal tensor decompositions. *SIAM J. Matrix Anal. Appl.*, 23:243–255, 2001.
- [44] T. Kolda and B. W. Bader. Tensor decompositions and applications. *SIAM Review*, 51(3):455–500, 2009.
- [45] D. Kressner, M. Steinlechner, and A. Uschmajew. Low-rank tensor methods with subspace correction for symmetric eigenvalue problems. *SIAM J. Sci. Comp.*, 36(5):A2346–A2368, 2014.
- [46] K. N. Kudin and G. E. Scuseria. Revisiting infinite lattice sums with the periodic fast multipole method. *J. Chem. Phys.*, 121:2886–2890, 2004.
- [47] C. Kweyu, M. Hess, L. Feng, M. Stein, and P. Benner. Reduced basis method for Poisson-Boltzmann equation. In: *Proceedings of VII European Congress on Computational Methods in Applied Sciences and Engineering*, 2016.
- [48] D. Lindbo and A.-K. Tornberg. Fast and spectrally accurate Ewald summation for 2-periodic electrostatic systems. *J. Chem. Phys.*, 136:164111, 2012.
- [49] F. Lipparini, B. Stamm, E. Cancès, Y. Maday, and B. Mennucci. Domain decomposition for implicit solvation models. *J. Chem. Theor. Comp.*, 9:3637–3648, 2013.
- [50] B. Z. Lu, Y. C. Zhou, M. J. Holst, and J. A. McCammon. Recent progress in numerical methods for Poisson-Boltzmann equation in biophysical applications. *Commun. Comp. Phys.*, 3(5):973–1009, 2008.
- [51] H. G. Matthies, A. Litvinenko, O. Pajonk, B. V. Rosic, and E. Zander. Parametric and uncertainty computations with tensor product representations. In: *Uncertainty Quantification in Scientific Computing, Springer Berlin Heidelberg*, pages 139–150, 2012.
- [52] I. V. Oseledets. Approximation of $2^d \times 2^d$ matrices using tensor decomposition. *SIAM J. Matrix Anal. Appl.*, 31(4):2130–2145, 2010.
- [53] I. V. Oseledets. Tensor-train decomposition. *SIAM J. Sci. Comp.*, 33(5):2295–2317, 2011.
- [54] E. L. Pollock and J. Glosli. Comments on P(3)m, FMM and the Ewald method for large periodic Coulombic systems. *Comp. Phys. Comm.*, 95:93–110, 1996.
- [55] A. Quarteroni, A. Manzoni, and F. Negri. *Reduced basis methods for parametrized partial differential equations: an introduction*. Springer International Publishing, 2015.
- [56] M. Rakhuba and I. Oseledets. Grid-based electronic structure calculations: the tensor decomposition approach. *arXiv:1508.07632*, 2015.
- [57] M. Stein, R. R. Gabdouliline, and R. C. Wade. Cross-species analysis of the glycolytic pathway by comparison of molecular interaction fields. *Molecular Biosystems*, 6:162–174, 2010.
- [58] F. Stenger. *Numerical methods based on Sinc and analytic functions*. Springer-Verlag, 1993.
- [59] J. Toulouse, F. Colonna, and A. Savin. Long-range-short-range separation of the electron-electron interaction in density-functional theory. *Phys. Rev. A*, 70:062505, 2004.
- [60] M. Zuzovski, A. Boag, and A. Natan. An auxiliary grid method for the calculation of electrostatic terms in density functional theory on a real-space grid. *Phys. Chem. Chem. Phys.*, 17:31550–31557, 2015.